

Article

Sedimentology and Paleodepositional Environment of the Early-Middle Miocene Tanjong Formation, Southeast Sabah: Evidence from Bulk Geochemistry and Palynology Analyses

Nur Faiqah Hisham and Nor Syazwani Zainal Abidin * 

Department of Geoscience, Faculty of Science and Information Technology (FSIT), Universiti Teknologi PETRONAS, Seri Iskandar 32610, Malaysia; nur_20000987@utp.edu.my

* Correspondence: norsyazwani.z@utp.edu.my

Abstract: Eight stratigraphic sections from well-exposed outcrops of the Early to Middle Miocene Tanjong Formation in the Kalabakan area, southeast Sabah, were investigated using an integrated approach, in which a comprehensive sedimentological facies analysis was linked with bulk geochemistry and palynological analyses. The integration of facies analysis, elemental CHNS, Fourier-transform infrared spectroscopy (FTIR), and palynological data provided a refined evaluation of the origin of organic matter (OM) and the reconstruction of the paleodepositional model. Seven facies associations were classified in the studied Tanjong Formation from 12 lithofacies components, interpreted as environments ranging from fluvial-deltaic to shallow marine: FA1—Floodplain, FA2—Fluvial channel, FA3—Coastal peat mires, FA4—Tidal flat, FA5—Delta front, FA6—Mouth bar, and FA7—Upper shoreface. Evaluation of the C/N ratio ranged between 4 and 48, and the total sulfur content ranged from 0.5 to 3. Elemental CHNS analysis suggests that the organic matter extracted from the coal and mudstone originated from terrestrial plants and fresh marine plankton. Accordingly, the three most prevalent FTIR spectra from the coal and mudstone samples were the OH- functional group stretching, the absorption spectrum of aromatic C=C stretching, and aromatic in-plane/out-of-plane C-H bending. Terrestrially derived organic matter within the examined samples was further validated by the predominance of aromatic compounds, and the palynological analysis indicated a back-mangrove freshwater pollen assemblage and a lower coastal plain setting proximal to the marine environment. The integrated findings from this research are vital in reconstructing a paleodepositional environment model that will improve the predictability of the petroleum system mechanisms and the future hydrocarbon potential for conventional petroleum exploration.

Keywords: facies analysis; facies association; fluvio-deltaic; shallow marine; depositional environment; Tanjong Formation



Citation: Hisham, N.F.; Zainal Abidin, N.S. Sedimentology and Paleodepositional Environment of the Early-Middle Miocene Tanjong Formation, Southeast Sabah: Evidence from Bulk Geochemistry and Palynology Analyses. *Minerals* **2023**, *13*, 494. <https://doi.org/10.3390/min13040494>

Academic Editor: Dominic Papineau

Received: 27 January 2023

Revised: 13 March 2023

Accepted: 14 March 2023

Published: 30 March 2023



Copyright: © 2023 by the authors. Licensee MDPI, Basel, Switzerland. This article is an open access article distributed under the terms and conditions of the Creative Commons Attribution (CC BY) license (<https://creativecommons.org/licenses/by/4.0/>).

1. Introduction

Sabah, located in northern Borneo, is bounded by the South China Sea to the west, the Sulu Sea to the northeast, and the Celebes Sea to the southeast (Figure 1). The complex tectonic setting of southeast Sabah has exposed various lithologies and associated sedimentary structures, indicating a range of depositional environments from continental (coals) to shallow marine cross-bedded sandstones and deep marine turbidites. However, these rock units exhibit weak fossil assemblages that limit available biostratigraphic information from foraminiferal or macrofossil species [1]. In general, previous studies on southeast Sabah have concentrated on its general geology [2,3], stratigraphy [1,4], geo-chemical and petrographical features of coal seams [5,6], and palynology [3]. The interaction between fluvial and marine processes has impacted the complex coastal plains and marginal marine environments, resulting in composite interbeds within the sedimentary facies. Thus,

integrated physical, geochemical, and biological investigations are necessary to unravel the rock record, which is vital for facies analysis. Elemental analyses of C, H, N, and total S were conducted to acquire information on the organic matter composition and determine whether the sample is from a marine or terrigenous source. The sulfur content in sedimentary rocks can provide significant insights into the activities of sulfur-reducing organisms and the organic matter's environmental settings and origin [7,8]. FTIR analysis is often used to distinguish the hydrocarbon functional groups in shale and coal [9], whereby the aromatic and aliphatic functional groups effectively evaluate the organic and inorganic minerals of coal or mudstone samples, in addition to deducing the depositional conditions [10–12]. Further palynological analyses provide essential information in identifying the type of plant, peat mire, climate, and sedimentation pattern of coal-bearing successions. The existence of palynofloral assemblages in coastal plains and marginal marine environments provides a mechanism to distinguish terrestrial, transitional, and fully marine deposits [13,14].

This study presents a systematic investigation of sedimentology, bulk geochemistry, and palynology based on the sedimentary successions and their stratigraphic correlation to the depositional environment of the onshore Tanjong Formation in southeast Sabah. Notably, these methods are commonly applied for a more accurate estimation in determining depositional conditions of coal-bearing sequences [15,16]. The implementation of in-depth facies analysis and facies association, as well as identification of the associated depositional processes from the evaluated sedimentological, bulk geochemical, and palynological characteristics, are aimed at (i) deducing facies successions and lithofacies classification of the Tanjong Formation, (ii) classifying the facies association and sub-depositional environment of the Tanjong Formation, and (iii) reconstructing a paleodepositional model for the Tanjong Formation. The findings from this study are vital for providing insight into the variations of sedimentary characteristics corresponding to varying sub-depositional environments of the Tanjong Formation.

2. Geology and Tectonic Setting

The northern part of Borneo, Sabah (Figure 1A), represents a complex geological history that has profoundly affected the regional tectonic evolution [17]. Five distinct tectonostratigraphic provinces were identified, separating the rock formations according to their age and lithology (Figure 1B): (a) an ophiolite complex or basement underlying the sedimentary succession of Sabah [18]; (b) Eocene-Lower Miocene sedimentary strata; (c) Early-Middle Miocene pyroclastic deposits [17]; (d) Middle Miocene chaotic deposits and melanges [19]; and (e) Early-Late Miocene shallow marine to fluvial-deltaic sediments [20]. The research area is restricted to the Early to Late Miocene tectonostratigraphic rock units, which are deformed into sub-circular to elliptical fault-bounded features known as the “circular basins” of Sabah [2]. In the central Sabah circular basins, notably on their western borders, the deep marine Oligocene Labang Formation was first deposited, followed by the Tanjong Formation deposits within a paralic, low-energy environment toward the basin depocenters during the Miocene [4].

Sabah lies in a tectonically active region whereby this area had experienced significant tectonic stress since the beginning of the Cenozoic, but the major tectonic event prevailed during the Miocene. A broad account of Sabah's tectonic evolution model is divided into six stages, ranging from Pre-Cretaceous to Holocene [17]. However, the Neogene Sabah Basin, the focus of this research, presumably began in the Late Eocene and experienced a structural event related to plate collision and extension with preceding sedimentation [21]. Shallow marine-deltaic clastics of the Tanjong and Kapilit Formations, which unconformably overlie the Kalabakan and pre-Neogene deep sediments, were continuously supplied to the NE up to the Sulu Sea by ongoing uplift in Central Borneo. Likewise, rifting of the Sulu Sea created East Kalimantan's extensional basin [22,23], which was previously affected by rifting of the Makassar Strait.

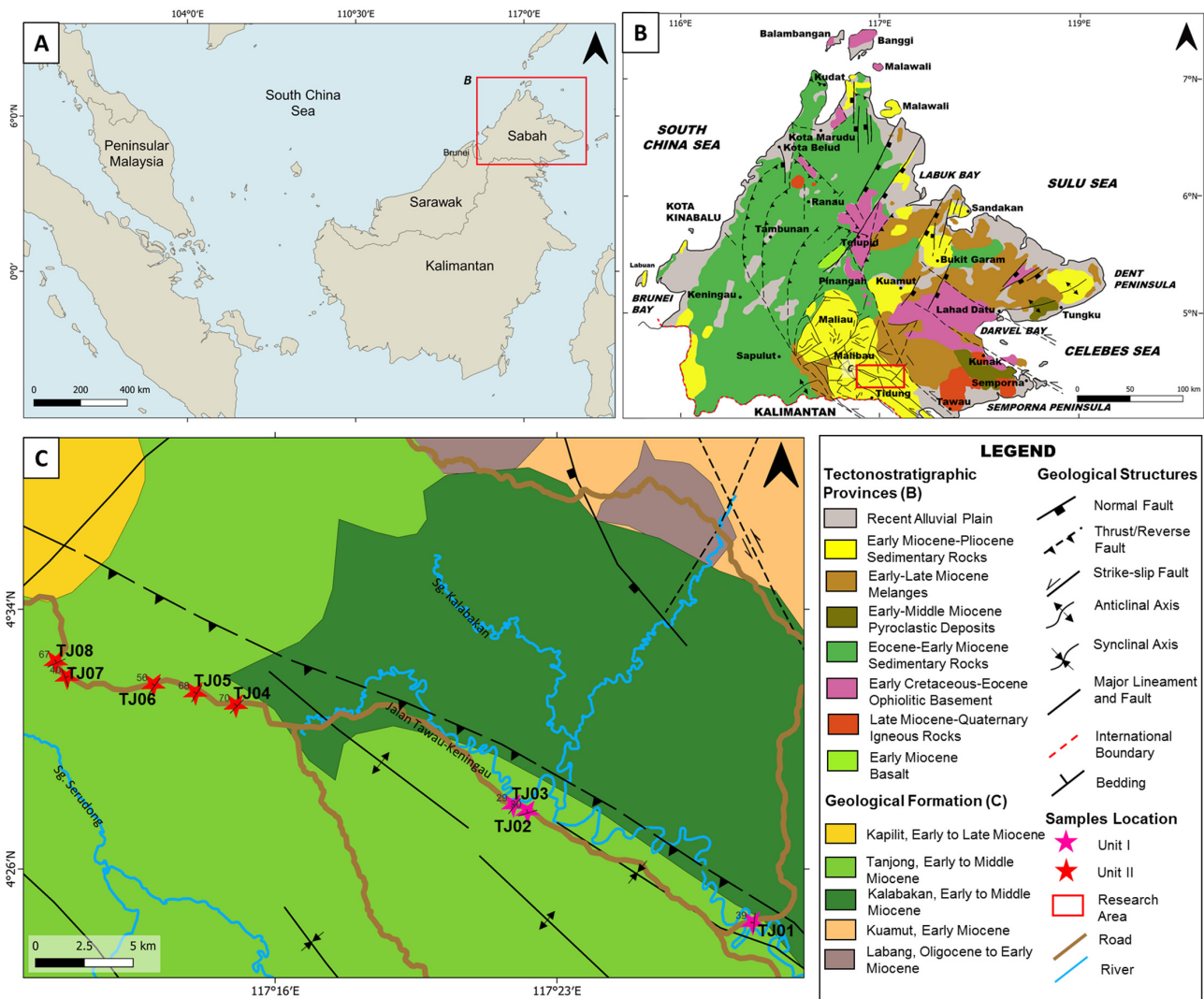


Figure 1. (A) Map showing the location of the study area. (B) Geological map of Sabah, modified from [24–26], showing the study area in south-to-southeast Sabah. (C) A close-up map showing the outcrop localities of the Tanjong Formation exposed in the study area.

The southern Sabah region primarily comprises exposed outcrops of clastic sandstone or mudstone, with the former commonly containing quartz arenites, and the latter being thinly-bedded and grey or black. The initial deposition of the Labang Formation, Kuamut Melange, and Kalabakan Formation was unconformably overlain by the syn-rift deposits of the Tanjong and later Kapilit Formations. An Early Miocene regional unconformity (Deep Regional Unconformity—DRU), corresponding to the Lower to Middle Miocene uplift, separates the Kuamut Formation and its associated melange unit from the overlying Tanjong Formation. The erosional event transitions Sabah from a deep marine setting with turbiditic sedimentation to a dominantly shallow marine setting [1]. The mud-dominated facies succession is prevalent in the northeast, signifying a progradational deltaic-to-shallow-marine environment. The respective stage of tectonic quiescence prevailed in the Late-Middle Miocene, suggested by the lack of syn-sedimentary structures in the Tanjong Formation [1,27]. The Tanjong, Kapilit, and Sandakan delta-plain deposits, which are composed of reefal facies overlain by deep marine clastic and thick sedimentation, resulted from a high burial thermal maturity during the Late Miocene eastern subsidence [28].

3. Study Area

The research area covers the Early to Middle Miocene Tanjong Formation in south-to-southeast Sabah (Figures 1C and 2). The formation includes extensive fresh outcrops in the Kalabakan area, specifically along the Tawau-Keningau roadcut. From the outcrops survey, eight well-exposed and nearly complete successions of the Tanjong Formation were chosen for an in-depth sedimentological study (Figures 3–5). The logged sections measure up to 92 m in stratigraphic thickness and present the first detailed sedimentological facies analysis of the Tanjong Formation within the Kalabakan area. It was challenging to precisely correlate the examined sections because of complex deformation, vegetation, and lateral facies changes. Based on the observed lithological characteristics, the siliciclastic sandstones and mudstones were prevalent in the Tanjong Formation outcrops and further subdivided into Lower Unit I (TJ01, TJ02, and TJ03) of mudstone-dominated facies with interbedded sandstone and mudstone, and Upper Unit II (TJ04, TJ05, TJ06, TJ07, and TJ08) of sandstone-dominated facies with the occupancy of coal seams. Heterolithic bedding comprising a mix of sandstone and mudstone composition and mud drapes was also typically observed within the outcrops, suggesting a tidal-influenced setting. The high amount of organic matter is indicated by the observed thinly laminated carbonaceous materials and dispersed coal lenses in most outcrops.

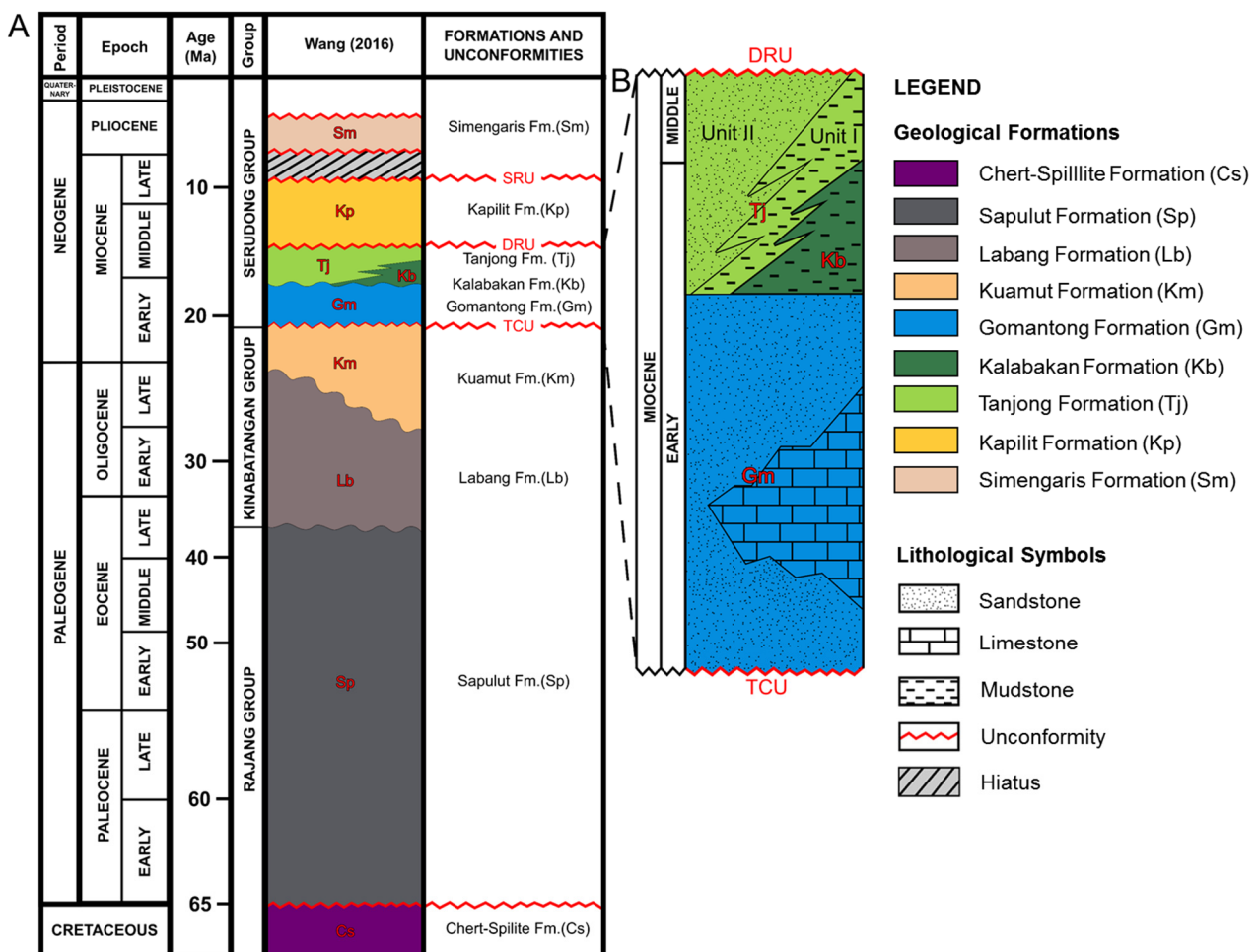


Figure 2. (A) General stratigraphic section of southern Sabah, modified from [1,29]. The red box indicates the studied rock formation. (B) Simplified stratigraphic framework for the onshore Early-Middle Miocene Gomantong, Kalabakan, and Tanjong Formation. Abbreviations: TCU—Top Croker Unconformity; DRU—Deep Regional Unconformity; SRU—Shallow Regional Unconformity.

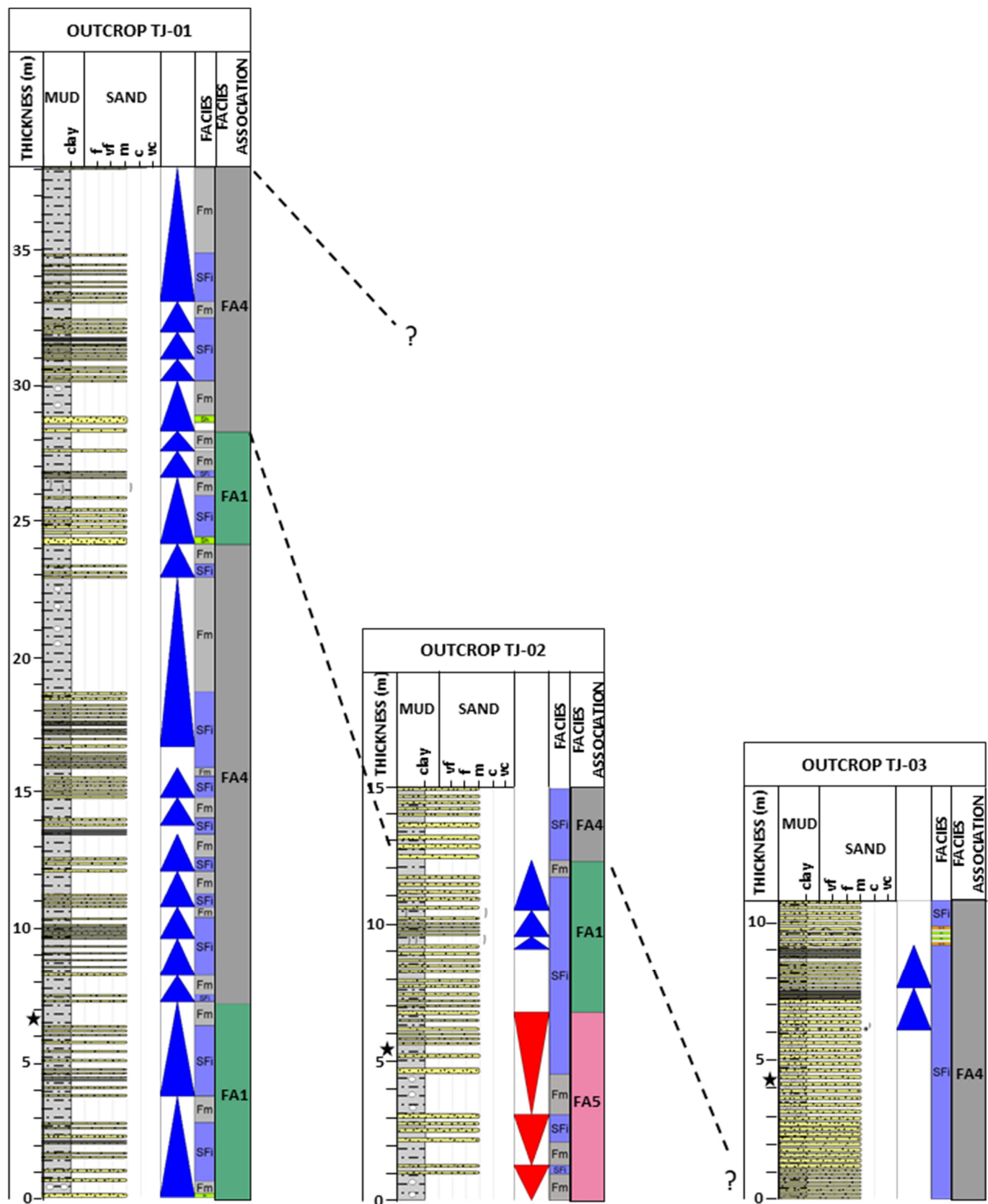


Figure 3. Sedimentary log successions with lithofacies, trace fossils, and facies association information in the studied outcrops of the Unit I Tanjong Formation.

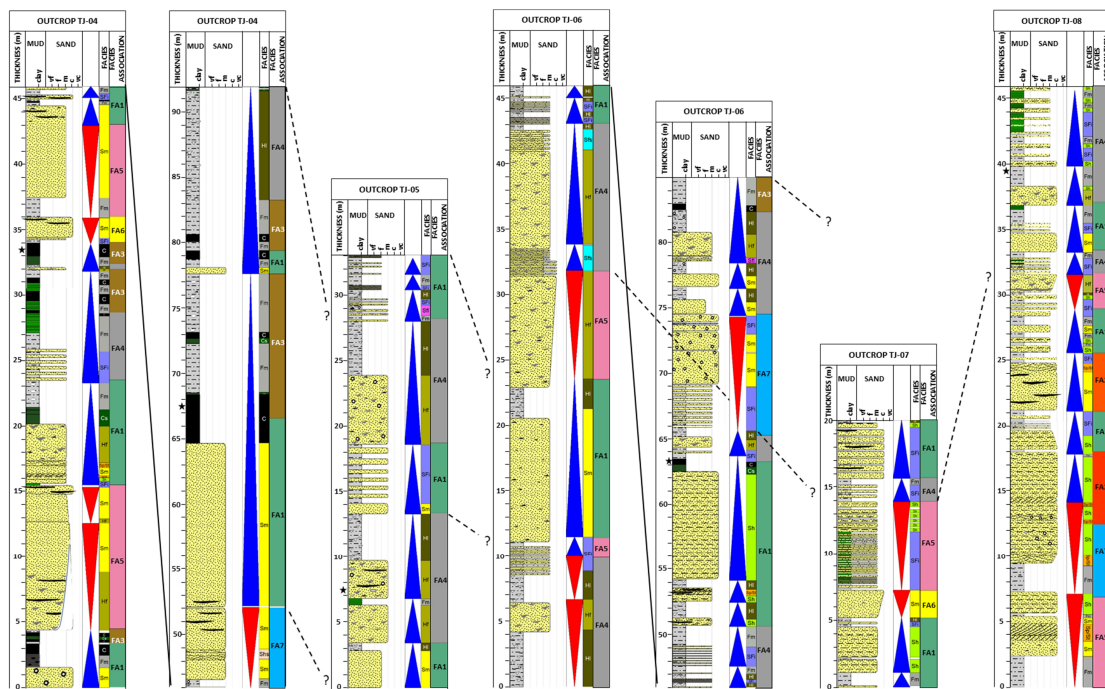


Figure 4. Sedimentary log successions with lithofacies, trace fossils, and facies association information in the studied outcrops of the Unit II Tanjong Formation.

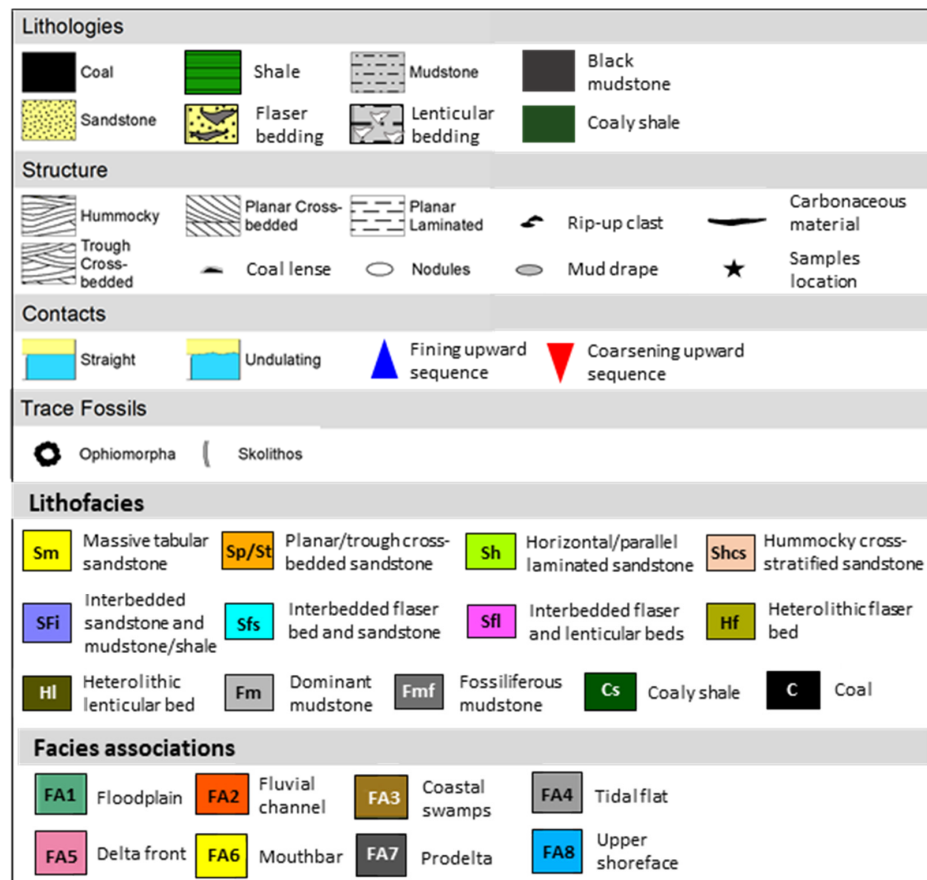


Figure 5. The symbols indicate sedimentary structures, lithofacies, and facies associations in the measured sedimentary log successions.

4. Materials and Methods

4.1. Sedimentary Facies Analysis

This research incorporated facies analysis on an outcrop scale to study and interpret sedimentary textures, sedimentary structures, trace fossils, and lithologic associations. Facies are identified and classified into facies associations in performing facies analysis. Understanding the context of how individual facies relate to one another is vital before establishing a depositional environment. Facies associations are assumed to be genetically or environmentally related due to the interpreted facies at the depositional setting, either vertically or laterally [30]. Moreover, facies associations are the fundamental components of facies analysis, comprising depositional elements representative of a particular depositional environment [31]. Hence, a comprehensive outcrop-based sedimentological facies analysis was conducted on the studied stratigraphic sections of the Tanjong Formation. Well-preserved sedimentary rock exposures of the Early to Middle Miocene Tanjong Formation along the Tawau-Keningau road provide important access for sedimentological facies analysis. A total of 13 mudstone and coal samples representing the Tanjong Formation were extracted from fresh, non-weathered, and well-exposed outcrops of the research study area. Contaminated and weathered surfaces were avoided during sampling to acquire a precise depiction of freshly exposed coal and mudstone samples in the Tanjong Formation. The facies analysis and facies association aimed to create a simplified facies scheme to interpret and differentiate the depositional settings of the formations in the research area.

A three-letter facies coding system was used to classify the lithofacies, with the first capital letter indicating the grain size and the second and third lowercase letters indicating the texture and sedimentary structures of the facies; the heterolithic facies is denoted with the letter “H” in this study [32]. Visual field identification of grain size and sorting of the beds was conducted utilizing a hand lens and a grain size comparator card. Facies associations were further identified from the classified lithofacies. Additionally, the mechanisms that controlled the transportation and deposition of the studied sedimentary successions were assessed. The physical characteristics of the sedimentary facies, as well as the observed biogenic structures and trace fossils, were incorporated with the findings from the bulk geochemistry and palynological analyses to interpret and validate the overall depositional environment.

4.2. Elemental (CHNSO) Analysis

Elemental or ultimate analysis of 10 mudstone and coal samples from the Tanjong Formation were analyzed for the elemental or ultimate carbon, hydrogen, nitrogen, and sulfur (CHNS) analysis. An Elementar VarioMicro CHNS analyzer with contemporaneous deduction of C, H, N, and total S was employed. Prior to the process, rock samples were crushed by manual crushing in a laboratory, as the instrument allows for a minimum 2 mg sample size and is based on a vertical furnace system. The four elements were simultaneously determined from a single weighed sample placed in tin foil, kept in the CHNS analyzer, and then qualitatively converted into carbon dioxide, water vapor, nitrogen gas, and sulfur dioxide, respectively. Each gas component was measured by infrared absorption after the separation of the gases. By deducting the total percentages of carbon, hydrogen, nitrogen, and sulfur from 100, the percentage of oxygen was obtained. Atomic H/C and O/C ratios, the C/N ratio, and other parameters were also calculated.

4.3. Fourier-Transform Infrared Spectrometer (FTIR) Analysis

Ten mudstone and coal samples from the Tanjong Formation were analyzed for the relative functional groups for FTIR analysis. FTIR spectroscopy was established as a method for the contemporaneous identification of organic and inorganic constituents, together with chemical bonds and organic contents, such as proteins, carbohydrates, and lipids. Pellets of 1 mg of crushed samples were prepared under the standard procedure [33], and they were ground up to a size of 75 mm using 100 mg potassium bromide (KBr). A PerkinElmer FTIR Spectrometer Frontier was used to gather the data. In FTIR analysis, the procedure

involves subjecting the samples to infrared (IR) radiation. The IR radiation affect the atomic vibrations of a molecule in the sample, which results in a particular energy absorption or transmission. Hence, the FTIR may help to pinpoint certain molecular vibrations that are present in the sample. The mid-IR absorbance mode with a wavelength resolution of 400 cm^{-1} to 4000 cm^{-1} was used to determine the FTIR pattern of the studied coal and mudstone samples.

4.4. Palynology Analysis

The organic-matter-rich deposits received significant consideration in palynology analysis because they are generally composed of well-preserved fossil palynomorphs. Seven organic-rich mudstones and coals in the Tanjong Formation were carefully sampled for palynological analysis. The samples were prepared and processed by following a recognized palynological workflow [34,35], with some modifications to enhance the palynomorph recovery. Firstly, the palynological samples were treated with hydrochloric (HCL) and hydrofluoric acid (HF) digestion and heavy liquid separation. During the process, the samples were washed and cleaned in distilled water to remove the contaminants and neutralize the conditions. The coal and mudstone samples, weighing around 10 g, were crushed using a mortar and pestle and broken up into fine equidimensional to angular pieces (approximately 1–2 mm in size). Next, a 24 h acid digestion process was performed on the crushed samples using 10% hydrochloric acid and 47% hydrofluoric acid for the dissolution of carbonates and silicates. The remnants were then treated with 2.0 SG of zinc bromide (ZnBr_2) for a heavy liquid separation technique to segregate the less dense organic materials from the heavy minerals. Then, 10% of potassium hydroxide (KOH) and 60% of nitric acid (HNO_3) were used to oxidize the lighter-floating organic residues. Canada balsam was used to mount the slides after they had been processed in polyvinyl alcohol. A Leica diaplan incident light microscope was used to examine the slides for qualitative and quantitative assessment from the successfully productive samples. At least 100 to 200 counts of recorded palynomorphs were present on each slide.

5. Field Observations

Facies Analysis

From the studied Tanjong Formation outcrops, eight vertical field sections with a stratigraphic thickness of up to 92 m were generated based on sedimentary logging of lithological composition, geometry, sedimentary, and biogenic structures (Figures 3–5). From the generated vertical field sections, twelve facies or lithofacies were discovered (Figures 6 and 7). Siliciclastic sandstone and mudstone rocks are the predominant lithofacies observed in the sedimentary sections, accompanied by thin coal seams. Massive tabular sandstone facies (Figure 6A) are prominently observed within outcrops of the Unit II Tanjong Formation (Figure 4), which include mud drapes, coal lenses, and carbonaceous material laminations. Additionally, horizontally laminated sandstone facies (Figure 6B,D) represent an interval of up to 8 m thick, as observed in outcrop TJ03, together with the presence of mud drapes, coal stringers, carbonaceous materials, and rip-up clasts (Figure 7C). Trough cross-bedded sandstone facies (Figure 6B,C) are predominately observed in outcrop TJ08, with minor occurrences in outcrops TJ04 and TJ06. Interbedded sandstone with mudstone or shale facies (Figure 6E) are commonly observed in outcrops of the Unit I Tanjong Formation. The coal-bearing sequence of thick-to-thin coaly shale and coal seams are observed in outcrops TJ04 and TJ06, respectively, (Figure 6F,G) ranging from approximately 0.90 m to 4 m thick. Along with the coaly shale and coal seams, structureless and carbonaceous mudstone-dominated facies are predominantly observed in all the outcrops with the presence of iron concretionary clasts (Figure 6H). The lithofacies is further classified by the presence of heterolithic (flaser and lenticular) bedding, composed of heterogeneous units of thin intermixed sandstone and mudstone (Figure 7A,B). Mud drapes, laminated carbonaceous materials, coal stringers, clasts, and lenses are typically observed within the heterolithic facies (Figure 7A,E). Low distribution of interbedded facies, comprising

heterolithic flaser and sandstone, are localized only in outcrop TJ06, while interbedded facies of heterolithic flaser and lenticular (Figure 7F) are localized in outcrop TJ05 and TJ06. A small-scale hummocky cross-stratified sandstone facies is observed in outcrop TJ04 (Figure 7G). Biogenic structures or trace fossils of *Skolithos* and *Ophiomorpha* are observed within mudstone-dominated and horizontal laminated sandstone facies, respectively (Figure 7D,H). The description and interpretation of the lithofacies are studied in order of significance to the understanding of the depositional environment (Table 1).

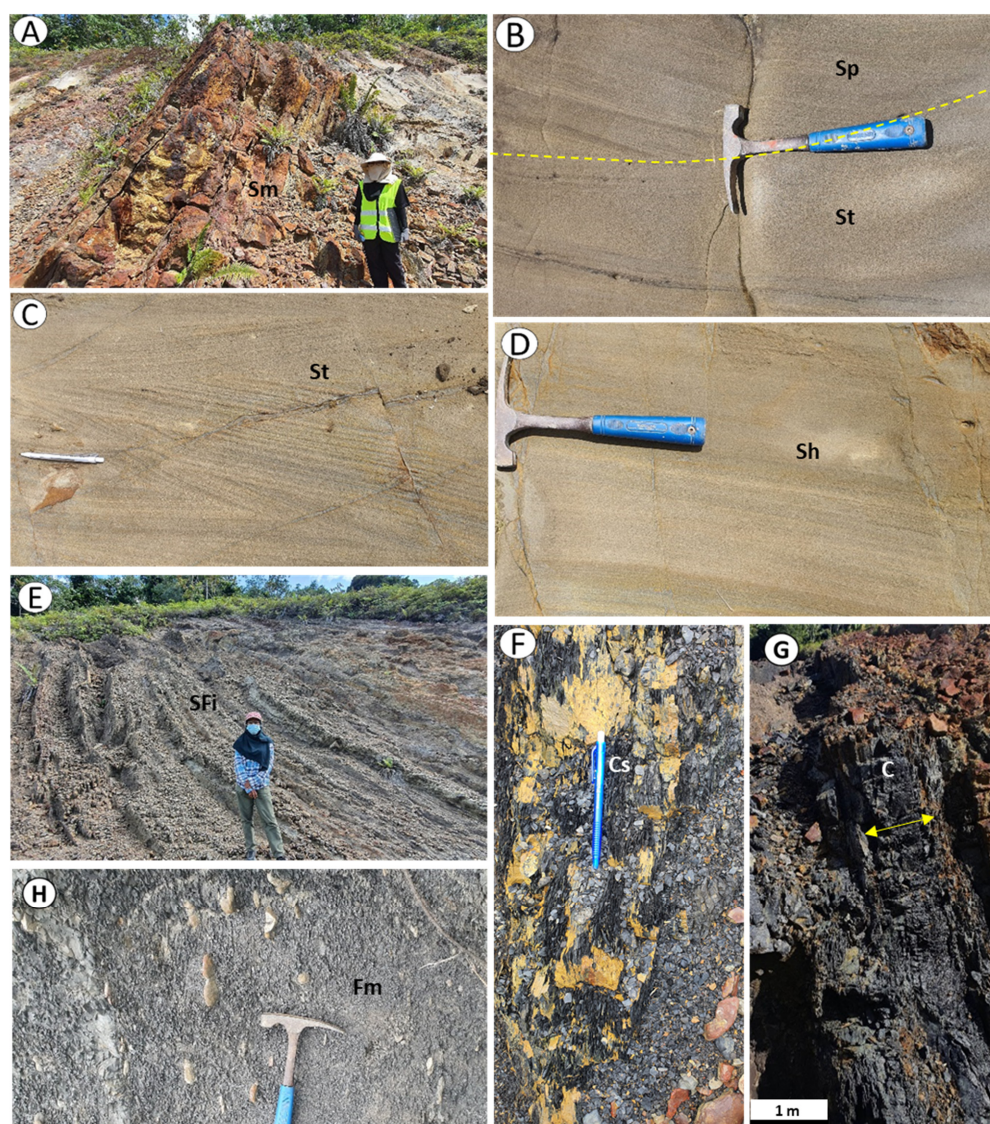


Figure 6. (A) Massive tabular sandstone facies (Sm) was observed in outcrop TJ06. (B) Planar cross-bedded sandstone (Sp) and trough cross-bedded sandstone (St) was observed in outcrop TJ06. (C) Trough cross-bedded sandstone (St) was observed in outcrop TJ08. (D) Horizontal or parallel laminated sandstone (Sh) in outcrop TJ08. (E) Thinly interbedded sandstone and mudstone facies (SFi) was observed in outcrop TJ05. (F) Coaly shale facies (Cs) with observed fissile characteristics in outcrop TJ04. (G) Thick coal seams (C) observed in TJ04. (H) Mudstone-dominated facies (Fm) with iron concretionary clasts observed in outcrop TJ01.

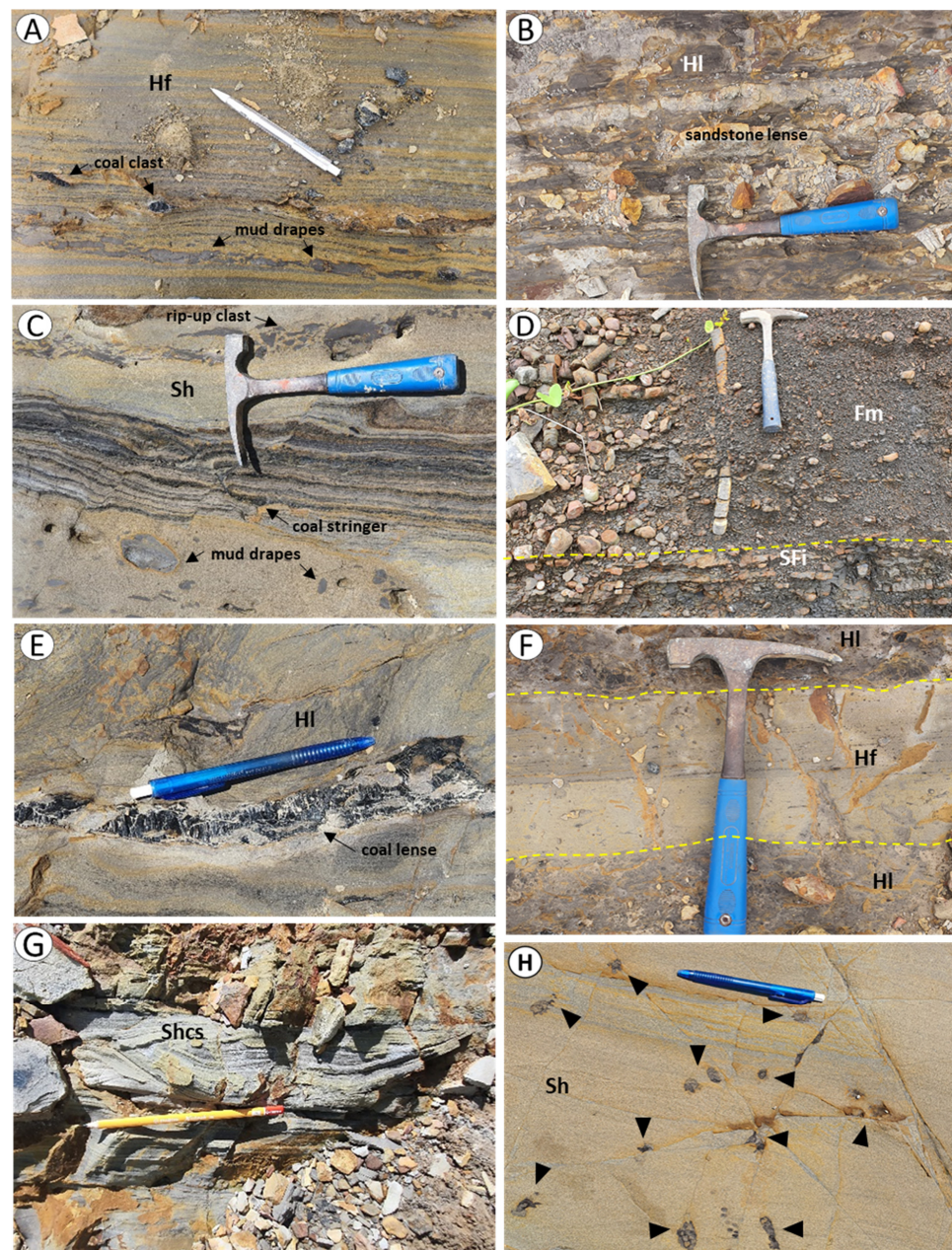


Figure 7. (A) Heterolithic flaser facies (Hf) with mud drapes and localized coal clast in outcrop TJ06. (B) Heterolithic lenticular facies (Hl) was observed in outcrop TJ04. (C) Laminated carbonaceous materials, thin coal stringers with mud, and rip-up clasts were observed in horizontal laminated sandstone facies of outcrop TJ06. (D) Vertical *Skolithos* trace fossil observed in outcrop TJ03. (E) Extensive coal lenses within heterolithic lenticular facies in outcrop TJ06. (F) Sharp to gradational contact of interbedded heterolithic flaser (light) and lenticular (dark) facies (Sfl). (G) Small-scale hummocky-cross stratification in sandstone (Shcs) found in outcrop TJ04. (H) Patches of *Ophiomorpha* trace fossils within the sandstone facies were observed in outcrop TJ08.

Table 1. The twelve (12) classified lithofacies in the Tanjong Formation, southeast Sabah.

No.	Code	Lithofacies	Descriptions	Trace Fossil	Interpretation
1	Sm	Massive tabular sandstone	Structureless and massive tabular medium-coarse-grained sandstone with sporadic pebbles. The sandstone varies from light brown to grey with a sharp bed contact (Figure 6A). The presence of laminated carbonaceous materials, coal lenses, and mud drapes can be observed within the beds. Hummocky cross-stratification occurs in one of the outcrops.	Possible Skolithos, Orphiomorpha	Internal stratification is absent in massive sandstone, implying that high-density turbidity currents decelerated quickly and abruptly came to an end [36,37].
2	Sp/St	Planar/trough cross-bedded sandstone	Planar and trough cross-bedded fine-medium-grained sandstone varies from light brown to grey color (Figure 6B,C). The bed contact differs from sharp to gradational. The presence of discontinuous carbonaceous laminations, coal lenses and stringers, and mud drapes is observed.	Possible Orphiomorpha	The planar/trough cross-bedded sandstone is supported by high-energy and unidirectional currents. These facies are developed from the migration of sinuous crested dunes in fluvial or river and tidal channels.
3	Sh	Horizontal/parallel laminated sandstone	Horizontal and parallel laminated fine-medium-grained sandstone with varying light brown to grey color (Figure 6D). The bed contact with other facies ranges from sharp to gradational. Sedimentary structures of laminated carbonaceous materials, coal lenses, mud drapes, and rip-up clasts were observed within the sandstone bed.	Possible Orphiomorpha	These facies are developed during flood conditions as an upper flow regime with high-energy currents. Planar lamination can also emerge as sediment deposition rates slow down, resulting from the recurring collapse of laminar-sheared layers at the base of a high-concentration flow [38].
4	Shcs	Hummocky cross-stratification	Medium-grained small-scale hummocky cross-stratified gray color sandstone with a relatively sharp contact (Figure 6G). These facies can only be found in the younger section of outcrop TJ05.	Absent	These amalgamated sandstone beds with small-scale hummocky cross-stratification serve as proximal storm beds with high-energy oscillatory and mixed flows during storms [39].
5	SFi	Interbedded sandstone and mudstone/shale	Thin to thick interbedding of fine- to medium-grained sandstone with mudstone or shale ranges from light brown to dark grey color (Figure 6E). Horizontal and parallel laminated sandstone is observed occasionally. In addition, laminated carbonaceous materials, coal lenses, and mud drapes can be observed in most of the outcrops. It displayed a sharp upper and lower contact.	Possible Orphiomorpha	The interbedded facies is believed to be deposited during high- and low-energy alternating currents, with mud deposition during slack-water intervals. The alternating sandstone and mudstone interbedded with the presence of mud drapes suggest a tidally influenced environment [40].
6	Sfs	Interbedded flaser beds with sandstone	Thin interbedding of fine-grained flaser bed with medium-grained sandstone bed in varying light brown to grey color. The flaser and sandstone beds have a gradational contact.	Absent	High- and low-energy currents occur periodically and alternately in tidal and seasonal settings with intervals of current or wave flows.
7	Sfl	Interbedded flaser beds with lenticular beds	Thin interbeds of heterolithic flaser and lenticular beds with gradational contact is observed to vary from light brown to dark grey color (Figure 7F).	Absent	High- and low-energy currents occur periodically and alternately in tidal and seasonal settings. Intervals of current or wave flows are commonly intermixed with slack-water periods.
8	Hf	Flaser heterolithic bedding	Fine-medium-grained sandstone is intermixed with mudstone, whereby the proportion of sandstone is higher than mudstone. The flaser bed sandstone is light brown, while the interlayered mudstone is grey (Figure 7A). It shows a gradational upper and lower contact. There is the presence of carbonaceous laminations, coal lenses, and mud drapes within the sandy matrix.	Absent	Heterolithic flaser facies deposited in varying hydraulic conditions during current intervals. The transportation of traction and deposition of rippled sandstone fluctuate with quiescence intervals of mud deposition [41].
9	Hl	Lenticular heterolithic bedding	A high proportion of mudstone is intermixed with fine- to medium-grained sandstone lenses (Figure 7B). The facies displayed a gradational upper and lower contact. The presence of carbonaceous laminations, coal lenses, mud drapes, and rip-up clasts is typically observed within the facies.	Possible Orphiomorpha, Echinoderm and Gastropod	Lenticular bedding is formed in conditions favoring the deposition and preservation of mudstone [42]. The sand deposits occurred during periods of current flow or wave action, with alternating slack-water conditions of mud deposition.
10	Fm	Dominant mudstone/shale	Structureless dark grey to black shale or mudstone of sharp contact with common carbonaceous laminations, coal lenses and stringers, mud drapes, and iron concretionary strata observed within the facies (Figure 6H).	Absent	Low-energy current flow with mud deposition in suspension. The significant concentrations of suspended sediment are formed by rapid deposition through flocculation.

Table 1. Cont.

No.	Code	Lithofacies	Descriptions	Trace Fossil	Interpretation
11	Cs	Coaly shale	Sharp contact of black-colored coaly shale that is a mixture of shale and coal mineral composition dominated by higher shale composition (Figure 6F). Coal lenses can be observed within the coaly shale.	Absent	In situ accumulation of plant material in coastal mires and flood plains.
12	C	Coal	Composed of dull to shiny black coal with prominently sharp contact (Figure 6G). Coals are highly fractured and contain undifferentiated plant residue.	Absent	In situ accumulation of plant material in peat mires, back-mangroves, coastal mires, and flood plains. Elevated water table with minimum current flow.

S—sandstone, F—Fines (silt-clay), m—massive/mudstone, p—planar cross-bedded, t—trough cross-bedded, h—horizontal-laminated, hcs—hummocky cross-stratified, i—interbedded, H—heterolithic, f—flaser, l—lenticular.

6. Results

6.1. Facies Association

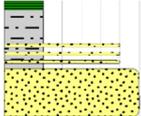
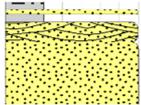
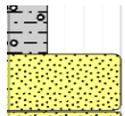
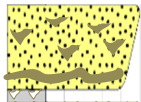
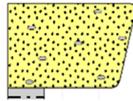
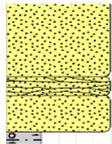
Facies associations and corresponding depositional characteristics were identified to provide greater insight into the sedimentary environmental processes incorporated in the research area. Seven main facies associations (FA) were identified through the integration of the sedimentary features from the outcrop loggings along the Tawau–Keningau road and also discrete lithofacies deduced from the facies analysis (Table 2). The facies associations include fluvial, deltaic, and shallow marine subenvironments. Detailed description and interpretation of each facies association are described in the following subsections. The seven facies associations—FA1, FA2, FA3, FA4, FA5, FA6, and FA7—are classified from twelve recognized lithofacies. Additionally, the FAs can be further classified based on the energy of sedimentary deposits, with the slow-energy deposits represented by FA1, FA3, and FA4, and the FA2, FA5, FA6, and FA7 indicating high-energy currents of varying coarse- to medium-grained massive sandstone deposits.

6.1.1. FA1: Floodplain Facies Association

Sedimentology: Medium- to coarse-grained sandstone facies (Sm, Sp/St, Sh), interbedded facies (SFi), mudstone (Fm), and coaly shale (Cs) or coal facies (C) with varying bed thicknesses are observed in this facies association. The observed massive tabular sandstone facies are thin- to thick-bedded (Figure 6A); small-scale planar cross-laminated sandstone facies (Figure 6B) and parallel laminated sandstone facies with mud drapes, coal lenses, and carbonaceous material laminations are also observed. This facies association displays a fining-upward sequence predominantly of fine-grained sediments. Heterolithic flaser and lenticular facies in outcrops TJ04, TJ05, and TJ06 indicate a deposition within a floodplain setting. The lower section of outcrop TJ06 exhibits the heterolithic lenticular or muddy facies capped by the thin coal facies. Rip-up clasts are observed within the heterolithic lenticular facies, while coal lenses of varying size and diameter are observed within the black mudstone facies.

Ichology: Bioturbation is sparse to absent. Concentrated *Ophiomorpha* trace fossil is observed within the heterolithic lenticular facies from outcrop TJ05, and vertical *Skolithos* trace fossil is observed in mudstone facies of outcrops TJ01 and TJ02. In the heterolithic lenticular facies from outcrop TJ06, a possible mold cast of gastropod and echinoderm is also visible.

Table 2. Facies association characterization (FA1–FA7) of the Tanjong Formation in southeast, Sabah.

Facies Association (FA)	Lithofacies	Description	Bioturbation	Interpretation
FA1 Floodplain	 Sm, Sp/St, Sh, SFi, Sfs, Hf, HI, Fm, Cs, C	Medium-coarse-grained sandstones which are thin to thickly bedded underlie the heterolithic and muddy facies and are overlaid by thin coal facies.	Absent to sparse, presence of Ophiomorpha and Skolithos trace fossils.	The cross-stratified sandstone and heterolithic interbedding facies indicate crevasse splay deposits, in which materials were deposited across floodplains after crossing the main channel.
FA2 Fluvial Channel-fill	 Sm, Sp/St, Sh, SFi, Fm	The trough cross-bedded sandstone is observed at the top of the massive tabular sandstone facies underlying the interbedded sandstone and mudstone or dominated mudstone facies.	Absent to sparse, presence of minor Ophiomorpha trace fossil.	These deposits, exhibiting an upward fining and thinning pattern, are suggestive of the river point bars anticipated in a fluvial or tide-influenced meandering channel.
FA3 Coastal swamps	 Fm, Cs, C	Dark grey shale to black mudstone, coaly shale, with varying carbonaceous organic materials.	Absent to intense	In situ accumulation of plant material in peat mires, back-mangroves, and coastal mires, possibly in fresh and brackish water.
FA4 Tidal flat	 Sm, Sp/St, Sh, SFi, Sfs, Sfl, Hf, HI, Fm	Medium-coarse-grained sandstones, heterolithic facies, and interbedded facies were overlain by carbonaceous shale and mudstone.	Sparse to moderate with the presence of Ophiomorpha and Skolithos trace fossils.	The dominant mud deposited in the intertidal to subtidal zones during intervals of slack water is suggestive of a deposition in alternating high- and low-energy currents.
FA5 Delta front	 Sm, Sp/St, Sh, SFi, Hf, HI, Fm	Composed of basal mudstone facies, heterolithic lenticular, wavy and flaser facies, interbeds of sandstone, and mudstone overlain by medium-coarse-grained massive sandstones.	Absent	The massive sandstone facies may be formed by strong currents flowing in the direction of the delta front's toe [43–45].
FA6 Mouth bar	 Sm, Sh, SFi, Fm	Thin mudstone as the base, followed by thin interbeds of sandstone and mudstone, capped by medium-coarse massive sandstone.	Absent	The associated facies point to sedimentation in a mouth bar setting, in which a direct supply of sand by terminal distributary channels takes place.
FA7 Upper Shoreface	 Sm, Sh, Sp/St, Shcs, Sfi, Fm	Primarily composed of medium-coarse-grained massive tabular and hummocky cross-stratified sandstone with thinly interbedded mudstone.	Sparse to intense with common Ophiomorpha trace fossils.	The hummocky cross-stratified sandstone is an indicator of storm influence deposited in the upper to lower shoreface shallow marine environment, typically above the storm-wave base [42,46].

Interpretation: The identified carbonaceous mudstones and thin coal seams indicate peat-mire conditions in a vegetated floodplain. The observed carbonaceous organic materials and undifferentiated plant materials in the mudstone facies caused the floodplain deposits to be composed of thinly interbedded sandstone and mudstone (SFi) facies, with paleosols manifesting surface processes. The observed sandstone facies is an indicator of energy variations during deposition. The cross-stratified sandstone and heterolithic interbedding facies indicate crevasse splay deposits, where the material was deposited across floodplains after crossing the main channel [47]. *Skolithos* trace fossil observed in the mudstone facies is believed to have formed due to an overbank avulsion and passively

infilled tracks from the coarser-grained facies of the floodplain setting. Suspension of mud deposits in extensive floodplains or inter-distributary channel embayments often supports the source and supply of fresh water with occasional marine incursions. The rare and concentrated *Ophiomorpha* trace fossil observed within the heterolithic lenticular facies supports the marine influence within the transitional floodplain to a tidally influenced setting. Additionally, the discovery of echinoderm and gastropod mold castings in the heterolithic lenticular facies from outcrop TJ06 implies an early stage of a tidal flat environment.

6.1.2. FA2: Fluvial-Dominated Channel Facies Association

Sedimentology: An erosional base of conglomeratic or trough-cross stratified sandstone facies constitutes the fluvial-dominated channel facies association with predominance of trough cross-bedded sandstone (St) (Figure 6C) [48]. Additionally, horizontally laminated sandstone (Figure 6D) is observed together with the medium- to coarse-grained massive tabular sandstone. This facies association forms a fining-upward sequence from the basal coarse-grained sandstone facies underlying the interbedded sandstone and mudstone (Figure 6E) to the mudstone or shale facies at the top. In the massive tabular sandstone facies, laminated carbonaceous materials were present. The fluvial-dominated channel facies association is commonly perceived in the sedimentary succession of outcrop TJ08 (Figure 4).

Ichtnology: Bioturbation is sparse to absent. The low distribution of the *Ophiomorpha* trace fossil is distinguished in the trough cross-bedded sandstone facies from outcrop TJ08.

Interpretation: Fluvial-dominated channel fill bodies are derived from freshwater rivers. The cross-stratified sandstones suggest that high-energy, unidirectional currents, resembling fluid flows or sediment gravity flows, were constrained to the fluvial channel for transport and deposition [48–51]. The associated deposits from this facies association exhibit an upward fining and thinning pattern, suggesting the river point bars anticipate a fluvial or tide-influenced meandering channel [52]. The observed trough cross-stratified sandstone facies represents the migration of three-dimensional dunes in the fluvial sediments [48,53–55]. The concentrated or monotaxic assemblages of the *Ophiomorpha* trace fossil within the trough cross-stratified sandstone further suggest the deposition in the distributary channels or fluvial channel fill facies association.

6.1.3. FA3: Coastal Peat Mire Facies Association

Sedimentology: The coal facies is predominantly observed specifically in outcrop TJ04 and TJ06, indicating a coastal peat mire facies association (Figure 4). This facies association comprises coaly shale (Figure 6F), coal seam of varying thickness from 5 cm to 2 m (Figure 6G), and carbonaceous mudstone facies. Thick, mud-dominated successions ranging from 1 m to 4 m, overlain by thin coal seams, typically rest on top of the floodplain and tidal flat facies associations (FA1 and FA4). Mudstone facies of darker greyish color found in this facies association indicate a high organic matter content. The insignificant distribution of sand and silt-size sediments supports the identified coastal peat mires setting. Coal and mudstone facies are observed prevalently at the upper succession of outcrop TJ04 while coaly shale overlain by thick coal seam facies of 90 cm is observed in outcrop TJ06 (Figure 4). Additionally, the presence of coal lenses and laminated carbonaceous materials are identified in the coaly shale facies from outcrop TJ06 as well as the possible in-situ iron oxide concretions in the mud-dominated facies (Figure 6H).

Ichtnology: Bioturbation is intense to absent.

Interpretation: The prevalence of fine-grained facies implies a deposition typically from a suspended fallout or low-energy current setting. The high occurrence of coal and carbonaceous facies suggests an accumulation of plant and organic materials under stable conditions. The low bioturbation degree verifies the low oxygen conditions in the coastal paleomire setting. The predominantly thick mud-dominated succession can be trapped and accumulated effectively, exhibiting the back-mangrove conditions within paleomires. As in Borneo, modern peat mires are found in back-mangrove conditions where freshwater

predominates and continuously covers the mire surface [56,57]. Additionally, brackish conditions could develop within paleomires as the seawater penetrated the back-mangrove environment. Due to the rising water table in parts of a peatland, peat accumulation and plant growth will be significantly hampered in the afflicted areas [58]. As a result, low-lying areas of the mire will be inundated, causing the deposition of clastic sediments, while peat accretion continues in the unaffected regions [58]. The thick coal seam, as observed in outcrop TJ05, could accumulate in the low-lying mires on coastal plains farther inland, in areas that are comparatively protected from storm surges and overbank flooding from rivers and tidal channels [59]. The intermittent structure, varying thickness, and the parting abundance of the coal facies further imply the transitional types of mires [60], which may indicate that portions of the mire complex were arbitrarily invaded by fluvial overbank debris or coastal flooding [59]. The intense bioturbation represented by the mottling of beds, possibly from undefined trace fossils, disrupted primary sedimentary structures.

6.1.4. FA4: Tidal Flat Facies Association

Sedimentology: The tidal flat facies association is commonly observed in all the studied outcrops, comprising a wide lithofacies variation, which includes sandstone-dominated, mudstone-dominated, heterolithic, and sandstone- and mudstone-interbedded facies. The heterolithic flaser and lenticular facies displayed varying sizes of sandstone lenses and mud drapes. The heterolithic bedding ranges from flaser to lenticular facies, indicating a fining-upward sequence. The heterolithic flaser facies, of high sandstone proportion (Figure 7A), exhibit bed thicknesses varying from 1 to 7 m that are gradationally underlying the muddy heterolithic lenticular facies (Figure 7B). Mud drapes, coal lenses, sandstone lenses, and carbonaceous material laminations are commonly found within the heterolithic facies (Figure 7C).

Ichtnology: Bioturbation is moderate to sparse. A low abundance of *Ophiomorpha* trace fossil within the heterolithic lenticular facies is only observed in outcrop TJ04, with moderate assemblages in the heterolithic flaser facies and massive sandstone facies of outcrops TJ05 and TJ06. Additionally, *Skolithos* trace fossil within the mudstone facies is only observed in outcrop TJ03 (Figure 7D).

Interpretation: The prevalent heterolithic flaser and lenticular facies with the occurrence of mud drapes and its associated trace fossil assemblages imply an overall tidal flat facies association. The dominant mud deposited in the intertidal to subtidal zones during intervals of slack water suggests deposition in alternating high- and low-energy currents. Tidal deposits may be identified by the presence of sand-mud doublets, rhythmites, and unidirectional deposits with reactivation surfaces. The changes from sand flats, and mixed flats to mud flats, presumably in the progradation parasequence, are represented by fining-upward successions on tidal flats [61,62]. In retrogradational parasequence, reverse grading is common, resulting in a coarsening-upwards trend from mud flats to sand flats, as shown in outcrop TJ06 (Figure 4). The interrelation of the stratigraphic location with other facies associations implies the sedimentation of mud flat, mixed flat, and sand tidal flat deposits in the upper to lower delta plain settings. The variety of grain sizes, from a sand flat to a mud flat, is also indicative of a deposit within an extensive tidal flat [63]. The identified coal lenses (Figure 7E) originated from the surrounding coastal peat mires and were carried by waves and currents onto the tidal flat, whereas the mud drapes were deposited at a high slack-water period [64,65]. *Ophiomorpha* and *Skolithos* trace fossil assemblages are rare in mudstone and sandstone, indicating that only a few species were able to survive and produce such imprints under stressed conditions [66]. During low tide (ebb) and high tide (flood), these stressed conditions are frequently present on the lower delta plain [67]. The low abundance of *Skolithos* vertical trace fossil is common in a higher energy zone of the tidal flat, while the tidal flat facies with merely *Ophiomorpha* trace fossil suggests a tidally exposed, stressed paleoenvironment with varying pore-water oxygenation.

6.1.5. FA5: Delta Front Facies Association

Sedimentology: The delta front facies association displays a coarsening-upward succession from the dominant mudstone, interbedded sandstone, and mudstone, heterolithic to the medium-coarse-grained massive tabular sandstone facies at the top. Laminated carbonaceous materials and coal lenses are observed within the heterolithic flaser facies (Figure 6E) with the presence of in situ iron concretions observed in the mudstone facies (Figure 6H). The sandstone beds comprised individual massive tabular sandstone (Sm), horizontal laminated sandstone (Sh), planar cross-bedded sandstone (Sp), and heterolithic flaser (Hf) facies. The heterolithic bedding displayed a coarsening-upward sequence from lenticular wavy to flaser facies (Figure 6F). Rhythmic mud drapes are commonly observed in cross-laminae and ripple patterns in the heterolithic flaser facies.

Ichtnology: Bioturbation is generally absent.

Interpretation: Significant supply of coarse-grained sandstone facies is observed in this facies association. The massive sandstone facies is believed to be deposited by the strong currents that move in the direction of the delta front's toe [43–45]. The presence of fine-grained heterolithic facies, together with a mixture of unidirectional or bidirectional current, wave, and tidal-influenced geological sedimentary structures are distinguished from the marginal-marine, mid-distal delta-front deposits [46]. As a result of the strong wave activity, fluid mud is formed in the delta-front environment, allowing for the resuspension of previous mud deposits, and later redeposited on top of the storm beds of a similar storm [68]. The lack of trace fossils is associated with lower heterogeneity (stressed conditions) or poorer dispersion of ichnofauna, supporting a freshwater or brackish influence during times of river flood into the delta-front environment.

6.1.6. FA6: Mouth Bar Facies Association

Sedimentology: Typically, this mouth bar facies association rests above the delta front facies association, forming a coarsening-upward sandy succession with thin basal mudstone facies. In the massive sandstone facies, mud drapes and laminated carbonaceous material are present. The massive sandstone facies, with thickness ranging from 2 to 6 m, is observed to wedge out, forming channel-like bodies (Figure 6A). As observed in outcrop TJ07, the mouth bar facies association is represented by the coarsening-upward sequence from the heterolithic lenticular facies of high mudstone proportion to the massive sandstone facies with mud drapes (Figure 4). In outcrop TJ04, a single coarse-grained massive sandstone facies with laminated carbonaceous materials suggests a deposit associated with the mouth bar.

Ichtnology: Bioturbation is generally absent.

Interpretation: The associated facies point to sedimentation in a mouth bar setting, in which a direct supply of sand by terminal distributary channels takes place. The fine-grained facies is absent, since the high and consistent river discharge transported the finer material farther from the river mouth. It is believed that the associated channel-like and laterally wedging-out sandstone facies represent mouth bar deposits on a subaqueous delta front with recurrent subaerial exposure [69]. This mouth bar facies association is considered to represent the deposit of a fluvial-dominated and tidally influenced mouth bar in possible brackish water conditions, from the predominance of current-generated facies, the combination of possibly fluvial and tide-generated facies, coarsening-upward facies succession, and lack of marine ichnofauna [70,71].

6.1.7. FA7: Upper Shoreface Facies Association

Sedimentology: Medium-coarse-grained massive tabular sandstones dominate this facies association, with laminated carbonaceous materials and thin mudstone interbeds. The massive tabular medium-grained sandstone exhibits hummocky cross-stratification (HCS), an indicator of the shoreface environment (Figure 7G). The upper shoreface facies association displayed a coarsening-upward succession from heterolithic lenticular facies, interbedded sandstone and mudstone facies, and hummocky cross-stratified sandstone

facies to the massive sandstone-dominated facies. The predominant massive sandstone facies range from 1 m to 5 m thick, and the hummocky cross-stratified sandstone facies of 1 m thick are observed in outcrop TJ04.

Ichnology: Bioturbation is intense to sparse, with a prevalence of *Ophiomorpha* trace fossil (Figure 7H), which occurs abundantly in the massive tabular sandstone facies and sparsely in the heterolithic lenticular facies.

Interpretation: The upper shoreface facies association is produced from a shallow marine environment, consistent with the predominance of wave and storm-generated deposits, traction current-generated deposits, and sandstone-dominated facies. Hummocky cross-stratified sandstone facies suggest a storm-influenced setting above the storm-wave base, with waning flow deposition reflected by the overlying symmetrical wave ripples [42,46,72,73]. Thick-bedded sandstone is an indicator of a high-energy winnowing process by transported currents during deposition. The high concentration of sandstone facies suggests a shoreward setting in which the fairweather wave action in shallow marine areas prevents the heavy suspended mud deposits. The prograding wave- or storm-influenced shoreline at a shallower subtidal shoreface zone may be represented by the FA7. The sedimentary structures of storm-influenced indication together with the *Ophiomorpha* trace fossils implied an environment in the upper shoreface [74,75]. The primary sedimentary structures are destroyed by the strong bioturbation, forming possible beds with mottling.

6.2. Bulk Geochemistry Analysis

6.2.1. Ultimate Analysis

Elemental or ultimate CHNS analysis of the selected samples indicates generally N-depleted organic matter in the mudstone and coal samples of the Tanjong Formation. Table 3 displays the ultimate analysis results acquired from eight mudstone and three coal samples of the Tanjong Formation. From the ultimate analysis, the examined mudstones record a very high O content (94.59–98.87 wt%) with an average of 97.15 wt%, while the coals contained a comparatively high C and O content, (32.36–73.5 wt%) and (17.02–63.51 wt%), averaging to 59.46 wt% and 32.83 wt%. The calculated O concentration is higher in the mudstone samples compared to the coal samples. The ultimate analysis data resulted in a high O and C content for both mudstone and coal samples, relatively moderate S (0.23%–3.42%), with an average of 1.41%, H (0.16%–4.84%) with an average of 1.51%, followed by low N content (0.11%–1.57%), with an average of 0.5%. The results of the calculated H to C (H/C) atomic ratio vary between 0.75 and 0.83 for coal samples and 2.69 to 26.65 for mudstone samples, while O to C (O/C) atomic ratio varies between 0.17 and 1.47 for coals and 28.87 to 200.63 for mudstones. The resulting H/C and O/C atomic ratios revealed that the mudstone samples contribute to higher H/C and O/C ratios than coal samples.

6.2.2. FTIR Analysis

The FTIR analysis was carried out to distinguish the minerals that are present in the mudstone and coal samples of the Tanjong Formation. Peak assignments were analyzed based on published literature [11–13,76–78]. The FTIR spectra of the Tanjong Formation mudstone and coal samples were determined in mid-infrared region absorbance mode at 450 cm^{-1} to 4000 cm^{-1} wavelength resolution (Figure 8). The mudstone and coal samples were analyzed for the different functional groups of hydrocarbons from FTIR analysis (Table 4). The spectra in most of the modalities displayed several band groups of organic matter and inorganic matrix, which include the hydroxyl compound (O-H stretch), saturated aliphatic (methyl and methylene stretch), and aromatic ring (aryl) for the organic matter bands. Additionally, the inorganic constituents comprise possible Si-O and Al-O bands, with mainly quartz clay minerals (e.g., illite, smectite, kaolinite), and iron oxide. Specifically, the Tanjong Formation mudstones revealed a prominent free hydroxyl O-H stretching at 3395.42 cm^{-1} to 3699.71 cm^{-1} , aromatic overtone and combination bands at

1870.63 cm^{-1} to 1880.21 cm^{-1} , aromatic C=C stretching, which is evident at 1630.09 cm^{-1} to 1648.17 cm^{-1} , further aromatic in-plane C-H bending, and aromatic out-of-plane C-H bending, which is detected in the range from 1028.79 cm^{-1} to 1033.36 cm^{-1} and 648.08 cm^{-1} to 915.48 cm^{-1} . Meanwhile, the possible inorganic constituents originating from Si-O-Al vibrations are represented by the bands at 3620.68 to 3699.71, 1031.43 to 1031.51, 912.72 to 915.48, 529.60 to 535.27, and 469.9 to 470.8, whereby the intense and broad bands at 3620.68 to 3699.71 could be attributed to kaolinite and illite minerals; Si-O or Al-O molecular vibration absorbance peaks range from 428.08 cm^{-1} to 535.27 cm^{-1} . Minor aliphatic C-H, CH_2 or CH_3 , and aliphatic ether stretching peaks are observed in low occurrence within the mudstone samples.

Table 3. Ultimate CHNS analysis with calculated oxygen of the studied mudstone and coal samples.

Sample ID	Lithology	Ultimate Analysis					Atomic Ratio		
		C (wt%)	H (wt%)	N (wt%)	S (wt%)	O (wt%)	H/C	O/C	C/N
TJ-01-mst	Mudstone	1.43	0.51	0.33	0.31	97.43	4.22	51.13	4.33
TJ-02-mst	Mudstone	0.70	0.16	0.18	0.47	98.50	2.69	105.59	3.81
TJ-03-mst	Mudstone	0.50	0.24	0.13	1.19	97.94	5.70	147.04	3.99
TJ-04-mst	Mudstone	2.46	1.05	0.11	1.79	94.59	5.08	28.87	21.70
TJ-04-coal (a)	Coal	72.51	4.55	1.57	3.42	17.95	0.75	0.19	46.21
TJ-04-coal (b)	Coal	73.50	4.84	1.53	3.10	17.02	0.79	0.17	48.14
TJ-05-mst	Mudstone	0.57	0.59	0.12	0.23	98.49	12.33	129.70	4.60
TJ-06-mst	Mudstone	0.37	0.35	0.12	0.29	98.87	11.40	200.63	3.16
TJ-06-coal seam	Coal	32.36	2.26	0.85	1.02	63.51	0.83	1.47	38.11
TJ-08-mst	Mudstone	1.80	0.65	0.20	2.58	94.77	4.29	39.51	8.87

C—Carbon, H—Hydrogen, N—Nitrogen, S—Sulfur, O—Calculated oxygen content = 100 – (C + H + N + S).

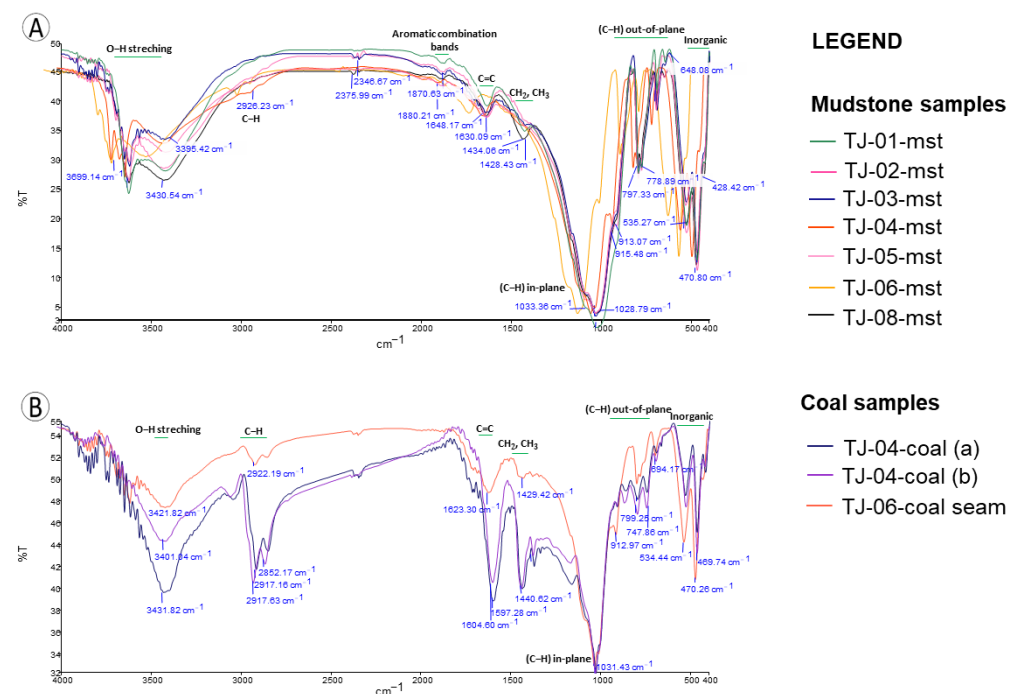


Figure 8. FTIR spectra of the (A) mudstone and (B) coal samples of the Tanjong Formation.

Table 4. Functional groups distinguished from FTIR spectra of the Tanjong Formation mudstone and coal samples.

Sample ID	Wavenumber (cm ⁻¹)														
	Free Hydroxyl	Saturated Aliphatic			Aromatic Ring Aryl					Inorganic Compounds					
	(O-H)	(C-H)	(CH ₂ , CH ₃)	Aliphatic Ethers	Aromatic Combination Bands	(C=C)	(C-H) in-Plane	(C-H) out-of-Plane	(Si-O)	(Mg, Al)-OH	(Al-O)	Illite, Smectite	Quartz	Quartz Silica	Iron Oxides
TJ-01-mst	3626.09–3422.84		1428.43		1873.2	1637.71	1028.79	828.99–648.08	1028.79		828.99	828.99, 3626.09	694.03, 3626.09	529.92–470.80	694.03–470.8
TJ-02-mst	3620.68–3422.03				1870.63	1648.17	1032.54	796.65–693.20				3620.68	693.20, 3620.68	531.20–470.60	693.20–470.6
TJ-03-mst	3621.53–3420.94				1871.17	1637.71	1031.51	796.42–648.23				3621.53	693.52, 3621.53	529.60–470.11	693.52–470.11
TJ-04-mst	3699.14–3411.60			1008.76	1872.75	1630.09	1033.36	913.07–694.71	1008.76			3699.14	694.71, 3699.14	535.27–470.47	694.71–470.47
TJ-04-coal (b)	3401.04	2917.63–2852.17	1440.41–1374.42			1597.28	1031.43	871.40–747.86			871.4			531.62–469.74	469.74
TJ-04-coal (a)	3431.82	2917.16	1440.62			1604.6	1032.14							534.75–470.44	470.44
TJ-05-mst	3696.93–3433.25				1875.21	1638.75	1032.68	915.48–694.01	915.48			3696.93	694.01, 3696.93	529.85–470.21	694.01–470.21
TJ-06-mst	3699.58–3433.85	2926.23				1638.56	1033.08	913.69–693.77				3699.58	693.77, 3699.58	530.48–470.25	693.77–470.25
TJ-06-coal seam	3421.82	2922.19	1429.42			1623.3	1032.41	912.97–694.17					694.17	534.44–479.26	694.17–479.26
TJ-08-mst	3699.71–3395.42			1008.3	1871.32	1637.3	1033.32	912.72–693.87	1008.30–912.72			3699.71	693.87, 3699.71	534.56–428.08	693.87–469.9

The coal samples of the Tanjong Formation are identified by broad OH stretching vibrations, which could also be attributed to H-O-H vibrations of adsorbed water present in the smectite clay minerals at 3401.04 to 3431.82 cm^{-1} [79], aliphatic C-H stretching peaks prominently at 2917.16 to 2852.17 cm^{-1} , aromatic C=C stretching peak ranges at 1597.28 to 1623.30 cm^{-1} , possible CH_2 or CH_3 stretching peaks at 1374.42 to 1440.62 cm^{-1} , aromatic in-plane C-H bending and aromatic out-of-plane C-H bending ranging from 1031.43 to 1032.41 cm^{-1} and 694.17 to 912.97 cm^{-1} , together with the possible inorganic constituents of either Si-O or mainly quartz and aluminosilicate minerals (e.g., clay and silicate minerals) vibration absorbance peaks evident at 1031.43, 912.97, 531.62 to 534.75, and 469.74 to 470.44 cm^{-1} . Additionally, the coal samples exhibit two peaks of asymmetric and symmetric C-H methylene stretching vibrations at 2930 cm^{-1} and 2840 cm^{-1} , respectively, on the shortwave shoulder of the broad OH continuum spectrum [80–82]. Aromatic overtone, combination bands, and aliphatic ethers are absent in the Tanjong Formation coals.

6.3. Palynology

The examined palynomorphs from the coal and mudstone samples of the Tanjong Formation are presented in the vertical frequency distribution of important taxa (Table 5). Palynomorph distribution is generally low in the examined samples, with a rich distribution being observed only in a limited number of horizons. The discovered palynomorph groups, comprising marine (aquatic) and continental (terrestrial) materials, support the tropical vegetation. Major palynomorphs from the genera *Sapotaceae* and *Stenochlaena* are recognized in coals from the Tanjong Formation, together with the recorded pteridophytic spores from the families *Cyatheaceae*, *Polypodiaceae*, and *Schizaeaceae*. The plants from these families suggest environments ranging from mires or marshy to subaquatic conditions. The analyzed palynomorph assemblages are of terrestrial palynofossils, indicative of a near-shore depositional setting [83]. Low pollen and spore assemblages characterize the coal samples with negligible taxa, originating from vegetated peat mire and riparian areas. The *Arenga* type, *Calamus* type, *Cyrtostachys*, *Dactylocladus* type, *Elaeocarpus* type, *Ilex* type, and *Pandanus*, as well as one grain of a rainforest species, the *Lithocarpus* type, and grass pollen from the *Gramineae* or *Poaceae* families were reported. In the upper section coal-bearing sample TJ-04b, only an individual grain of *Florschuetzia trilobata* was found, making it hard for the relative age dating identification without any supporting marker pollen. Moreover, the vitrinite equivalent blackish-dark phytoclasts dominate the coal samples.

The palynomorph assemblages in the mudstone samples of the Tanjong Formation are higher than in coal samples. The total assemblage was dominated by angiosperm pollen from the families *Caesalpiniaceae*, *Gramineae* or *Poaceae*, *Magnoliaceae*, *Papilionaceae*, *Proteaceae*, *Rhizophoraceae*, *Rubiaceae*, and *Sapotaceae* in the mudstone samples. The *Avicennia* type, *Rhizophora* type, and *Florschuetzia* type (*Florschuetzia trilobata* and *Florschuetzia levipoli*) mangrove-to-bac- mangrove assemblages suggest a brackish setting [84]. The coastal peat mire species *Alchornea*, *Barringtonia*, *Blumeodendron*, *Calophyllum* type, *Casuarina* type, *Dactylocladus* type, *Elaeocarpus* type, *Gonystylus* type, *Pometia*, and *Stemonurus* are examples of those that belong to the hinterland group. A single pteridophytic spore was represented by *Laevigatosporites* sp. (*Schizaeaceae*) in mudstone sample TJ-01. Additionally, riparian components from the *Myrtaceae* family, *Pandanus*, and *Ilex* type are recorded in the examined samples. The recognized *Florschuetzia* group pollens, originating from the mangrove genus *Sonneratia*, including the *Florschuetzia levipoli* (*Sonneratia caseolaris*) and *Florschuetzia trilobata*, act as a significant indicator in dating Miocene sedimentary deposits, particularly within Borneo and its surrounding regions, suggesting an age within the Early to Middle Miocene [57].

Table 5. Distribution chart showing palynomorphs species of the analyzed coal and mudstone samples in the Tanjong Formation.

Sample ID	Lithology	Lithofacies	FA	Mangrove/Back Mangrove					Hinterland																	Spores			Seasonal/Montane								
				<i>Avicennia</i> type	<i>Florschuetzia levipoli</i>	<i>Florschuetzia trilobata</i>	<i>Florschuetzia</i> type	<i>Rhizophora</i> type	<i>Alchornea</i>	<i>Areniga</i>	<i>Barringtonia</i>	<i>Blumeodendron</i>	<i>Casalpinniaceae</i>	<i>Calamus</i> type	<i>Calophyllum</i> type	<i>Casuarina</i> type	<i>Cyrtostachys</i>	<i>Dactylocladus</i> type	<i>Elaeocarpus</i> type	<i>Gonystylus</i> type	<i>Ilex</i> type	<i>Lithocarpus</i> type	<i>Magnoliaceae</i>	<i>Myrtaceae</i>	<i>Pandanus</i>	<i>Papilionaceae</i>	<i>Pometia</i>	<i>Proteaceae</i>	<i>Rubiaceae</i>	<i>Sapotaceae</i>	<i>Stemomurus</i>	<i>Cyathidites</i> sp. (<i>Cyathaceae</i>)	<i>Laevigatosporites</i> sp. (<i>Schizaceae</i>)	<i>Polydiisporites</i> sp. (<i>Polyodiaceae</i>)	<i>Verrucatosporites usmensis</i> (<i>Stenochlaena</i>)	<i>Alnus</i>	<i>Graminae/Poaceae</i>
TJ-01	Mudstone	Fm	Floodplain	1		1	2	1							1		1				1	1		1	1	1					1				1	1	
TJ-02	Mudstone	SFi	Tidal flat				1																														
TJ-03	Mudstone	SFi	Tidal flat	2	1		3	1		1	1			2	1		1				1	1	1			1	2	1									
TJ-04a	Coal	C	Coastal peat mire													1																					
TJ-04b	Coal	C	Coastal peat mire		1										1	1	1						1				1					1			2		
TJ-05	Coal	Hf	Tidal flat						1					1															1	2	1	2					
TJ-06	Coal	C	Coastal peat mire											1					1											1						1	

7. Discussion

7.1. Organic Matter Origin

Based on the CHNS analysis, the sulfur concentrations (S wt%) for coal and mudstone samples ranged between 1.02–3.42 and 0.23–2.58, respectively, indicating the varying degrees of marine influence on the organic matter of Tanjong Formation sediments. Rocks formed in reducing, hypersaline marine environments generally contain higher sulfur concentrations, while rocks with lower sulfur content are likely formed in freshwater lacustrine settings [85,86]. The low sulfur content and overall diagenetic environment of the Tanjong Formation mudstone deposits suggest sulfate-reducing conditions associated with deposition in marginal marine and brackish water [87]. The organic matter origin of the Tanjong Formation deposits was determined using organic C/N ratios. High C/N ratios of 21.7 for mudstone and 38.11–48.14 for coal suggest the origin from terrestrial plants or fresh land-derived organic matter. The high C/N ratio may be due to the preferential nitrogen loss in organic matter derived from phytoplankton through suboxic diagenesis or could be an indicator of an initial composition of terrestrial organic matter. Additionally, low C/N ratios for the Tanjong Formation mudstones ranged between 2.48 and 8.87, suggesting that the organic matter was either unaltered algal organic matter or marine plankton [88,89]. This implies that the organic matter in the Tanjong Formation mudstone originated from algal marine plankton of a sulfate-reducing environment, with some influence from the freshwater setting, based on the integrated sulfur concentrations and C/N ratio. Furthermore, the organic matter for the Tanjong Formation coals has a considerable degree of marine influence, indicating that it originated from fresh land-derived or terrestrial plant settings.

Numerous studies have emphasized the importance of using FTIR techniques to rapidly and accurately quantify the organic and mineralogical components of coal [90,91], shale [92,93], and other sedimentary rocks. Since organic matter functional groups reveal the majority of their distinctive vibration modes in the IR spectral region, FTIR techniques can be used to gain quantitative findings on the mineral compositions of geological rock samples [94]. The amount of material present is correlated with the peaks of the graphs produced by this study. The FTIR spectra of the Tanjong Formation mudstone and coal samples (Figure 8) show the dominance of aromatic compounds, which include the aromatic overtone and combination bands, aromatic C=C, aromatic C-H in-plane, and aromatic C-H out-of-plane bending peaks. The predominance of aromatic compounds supports the terrestrial origin of organic matter in the Tanjong Formation coals. In contrast to coal, mudstone typically exhibits weaker vibration bands of aliphatic C-H at 2800 to 3000 cm^{-1} in the infrared spectrum. Minor occurrences of aliphatic compounds, such as the aliphatic C-H bending peaks, are observed within all the coal samples, while the aliphatic ether bending peaks were observed within mudstone samples TJ-04-mst and TJ-08-mst.

Additionally, absorbance peaks in the OH⁻ stretching vibration are prominent in all spectral groupings from 3620.68 cm^{-1} to 3699.71 cm^{-1} , which are associated with quartz, phyllosilicates kaolinite, or clay mineral constituents [79,95], such as illite and smectite minerals [96,97]. Validation from the accompanying bands ranging from 1870.63 cm^{-1} to 1880.21 cm^{-1} indicates similar contributions of quartz and illite or smectite minerals [98,99]. The dominant overtone bands in quartz and silica, and the primary bending vibrations of water absorption corresponded to the bending peaks ranging from 1597.28 cm^{-1} to 1648.17 cm^{-1} [100]. The bands between 1028.79 cm^{-1} and 912.72 cm^{-1} correspond to Si-O of clay and quartz minerals, followed by the (Mg, Al)-OH vibrations in clay minerals dominating the bands at 915.48 cm^{-1} [101]. The peaks at 828.99 cm^{-1} and 871.40 cm^{-1} correspond to vibrations of Al-O in clay minerals. The identification of illite and smectite minerals is indicated by the low concentration but steady peaks at 828.99 cm^{-1} [99]. Additionally, the mid-IR subregion, between 800 cm^{-1} and 400 cm^{-1} , comprises the highest prominent quartz lattice vibrations, with the dominant quartz band ranging from 693.20 cm^{-1} to 694.71 cm^{-1} , and is well-resolved to provide primary information on the quartz of the inorganic matrix. Quartz silica linked to the influenced SiO molecular vibra-

tions from 428.08 cm^{-1} to 535.27 cm^{-1} is also found in the mudstone and coal samples [102]. Nearly all the samples exhibit bands between 469.74 cm^{-1} and 694.71 cm^{-1} , which is most likely related to iron oxides. The predominance of Si-O and Al-O indicates kaolinitic-rich rocks formed in warm and semi-arid conditions. Comparably, coal accounts for a significant portion of the quartz and kaolinite composition. The high aromatization and humification processes allow for stronger polymerization with increasing molecular weight [103], which validates the kerogen type III origin with humic and terrestrial contribution from higher plants that produce “aromatic” pyrolysates. Overall, the interpretation from bulk geochemical analyses indicates the source of organic matter from terrestrial to shallow marine environments, with a predominance of kerogen type III gas-generating potential, rich in aromatic compounds and adequate aliphatic compounds for the Tanjong Formation samples.

7.2. Paleodepositional Environment Model

The integrated sedimentological facies analysis, ichnological analysis, bulk geochemical and palynological analyses of the Tanjong Formation deposits displayed a predominance of fine-grained sedimentary facies composed of the floodplain, tidal flat, and delta front facies associations in the lower section. The middle section predominated in coal seams indicative of a coastal peat mire facies association, while the upper section comprised coarse-grained dominated facies of the fluvial channel fill, mouth bar, and upper shoreface facies associations. The relationship between the river, wave, and tide actions is considerable, as shown by the facies associations of varying depositional systems. The wave and tide processes contribute to the higher distribution involving the FA3, FA4, FA5, FA6, and FA7, in comparison with the minor distribution of the river process in FA1 and FA2 of fluvial deposits. The overall paleodepositional model from fluvial deltaic to shallow marine sub-environments of the Tanjong Formation (Figure 9) is characterized by channelized fluvial tidal flats ranging from sand flats to mud flats, delta front comprising mud-dominated and heterolithic (flaser and lenticular) facies, and sand-dominated facies in the mouth bar and upper shoreface, with predominated coal facies of coastal mires. The salt marsh deposits evolved further inland, while deposited sediments from intertidal flats formed close to the basin margin [104]. The subtidal extension of nearby mangrove and tidal flat sub-environments is also developed by the low-energy traction and suspended tidal flat deposits. The coarse sandstone matrix of heterolithic flaser facies partly represents the delta plain and delta front, while the vertical sequence of the fluvial-tidal sandstone and heterolithic facies represents a pro-gradational delta succession. The vertical sequence of mouth bars, fluvial channel fills, and tidal bars is considered to be deposited in distributary channels. The vertical succession trends from the coarse-grained upper shoreface into the fine-grained coastal mires are thought to represent the landward shallowing of the environment. From the sedimentary log succession, outcrop TJ04 exhibited the almost full range of facies associations (FA1, FA3, FA4, FA5, FA6, and FA7), transitioning from a sandstone-dominated delta front, mouth bar, and concentrated hummocky cross-stratified sandstone facies of the upper shoreface to a mudstone-dominated floodplain and tidal flat, overlain by occasional coastal peat mires and/or back-mangrove settings.

Four coal and three mudstone samples from the palynological investigation revealed a transition from mangrove to back-mangrove and/or coastal peat mire settings (Table 5), of which the specific stratigraphic sampling points were recorded in the sedimentary logs (Figures 3–5). The abundance of the Rhizophoraceae family in the palynomorph assemblage indicates mixed-mangrove source vegetation. Moreover, a low distribution of palynotaxa in the coal samples constitutes freshwater palynomorphs from peat mires and riparian vegetation beyond the tidal-limited zone. Additionally, the mudstone samples of the Tanjong Formation indicated peat mire, coastal, and riparian plant species, denoting a lower coastal plain close to the marine setting. The mangrove and back-mangrove palynomorph assemblages identified in the coaly horizon are also conceivable as a transition from tidal mud flats into coastal peat mires. The recorded palynomorphs from the families Cyatheaceae, Polypodiaceae, Schizaeaceae and Caesalpiniaceae, Magnoliaceae,

Papilionaceae, Proteaceae, Rhizophoraceae, Rubiaceae, and Sapotaceae in both coal and mudstone samples point to the vicinity of the terrestrial source (fluvio-deltaic systems) connected to the lower energy of a shallow marine setting [105,106]. Overall, the identified palynoflora corresponds to the transition between freshwater peat mire to coastal mangrove, with precursor peat that could be accumulated under freshwater or oligohaline peat mires within back-mangrove conditions.

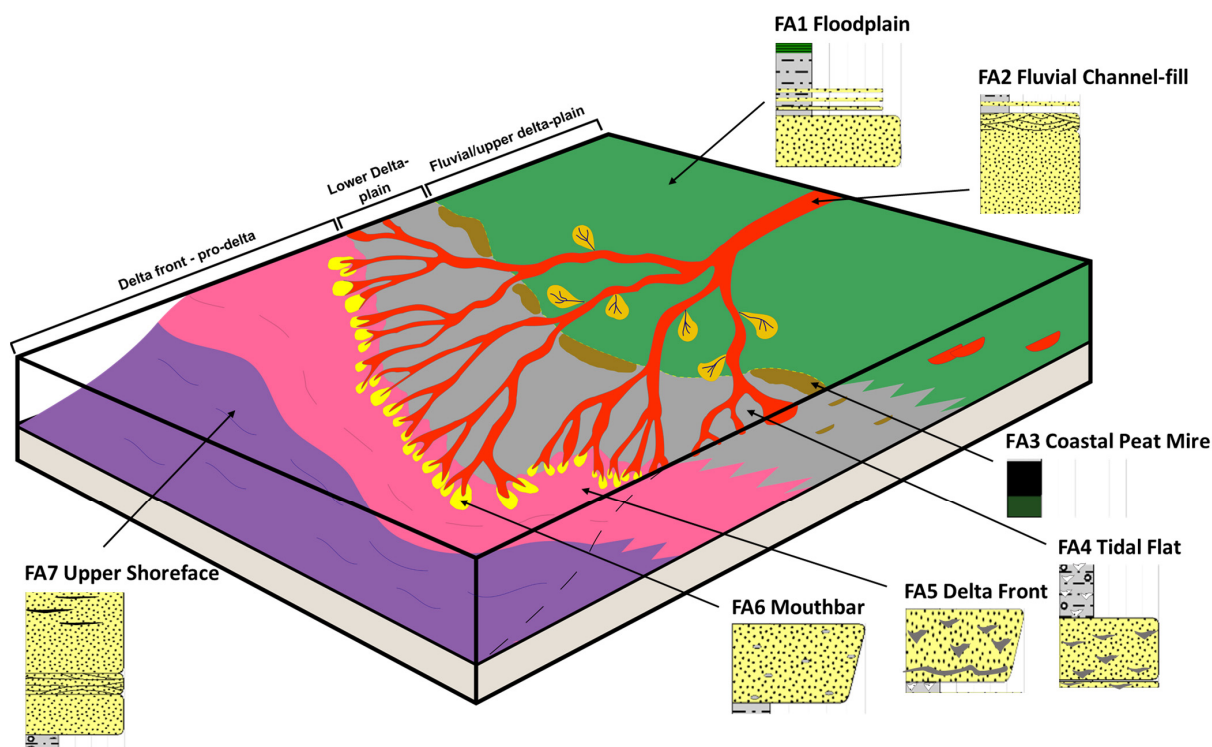


Figure 9. Paleodepositional model for the studied Tanjong Formation with different sub-environments from FA1 to FA7.

8. Conclusions

This study combined an integrated sedimentological, bulk geochemical, and palynological analysis of the Tanjong Formation coal and mudstone facies to determine the organic matter origin, mineral composition, and environmental conditions for reconstructing the paleodepositional model. Based on the in-depth sedimentological facies analysis, twelve lithofacies were identified and further grouped into seven facies associations, consisting of sub-environments ranging from the floodplain, fluvial channel fill, coastal peat mire, tidal flat, delta front, and mouth bar to the upper shoreface. The organic matter origin and its mineral composition were well defined by the interpreted elemental CHNS and FTIR analysis. The low sulfur content and high C/N ratio of the Tanjong Formation mudstones indicate that most of the organic matter originated from algal marine plankton in a sulfate-reducing environment, suggesting a freshwater lacustrine setting. Conversely, the organic matter extracted from the coals had a greater marine influence, postulating an origin from terrestrial plants or fresh land-derived settings. The dominance of aromatic compounds from the FTIR spectra with the presence of inorganic compounds, such as quartz, kaolinite, illites, and smectites minerals, suggest the potentiality of organic materials originating from terrestrial settings and corroborates the findings from the CHNSO analysis.

The distribution chart of identified palynomorphs species is characterized by high occurrences of pollen with an affinity for mangrove to back-mangrove settings, i.e., *Avicennia*, *Florschuetzia*, and *Rhizophora*, in the Tanjong Formation mudstones. Meanwhile, a freshwater or coastal peat mire setting is marked by *Arenga*, *Cyrtostachys*, *Elaeocarpus*, and *Gramineae* in the Tanjong Formation coals, indicative of the transition from mangrove to

back-mangrove and coastal peat mire settings. In conclusion, the reconstructed paleodepositional model of the Miocene Tanjong Formation deposits spans transitional fluvial, deltaic, and shallow marine environments.

Author Contributions: All authors have contributed to the writing and editing of this article. Writing original draft preparation, N.F.H.; supervision, N.S.Z.A.; writing, review and editing, N.S.Z.A.; Visualization, N.F.H.; funding acquisition, N.S.Z.A. All authors have read and agreed to the published version of the manuscript.

Funding: Special acknowledgment is given to the Yayasan Universiti Teknologi PETRONAS (YUTP) for supporting the fund under the university's internal grant (YUTP-FRG 015LC0-305).

Data Availability Statement: Data sharing is not applicable to this article.

Acknowledgments: This research work serves as the first author's Master's degree project at Universiti Teknologi PETRONAS. Hence, the authors appreciate the time and effort of the respected reviewers and editors for their positive reviews and recommendations in improving the quality of the manuscript. The authors would also like to convey a heartfelt appreciation to the Geoscience Department at Universiti Teknologi PETRONAS for providing the analytical facilities and assistance in the completion of this research.

Conflicts of Interest: The authors declare no conflict of interest.

References

- Balaguru, A.; Nichols, G.; Hall, R. Tertiary stratigraphy and basin evolution, southern Sabah: Implications for the tectonostratigraphic evolution of Sabah, Malaysia. *Geol. Soc. Malays.* **2003**, *47*, 27–29. [[CrossRef](#)]
- Balaguru, A. Geology and mineral resources of the Sungai Kalabakan area, Malibau, Sabah. *Geol. Surv. Malays. Sabah* **1996**, Syit 41117/5.
- Hutchison, C.S. *Geology of North-West Borneo: Sarawak, Brunei and Sabah*; Elsevier: Amsterdam, The Netherlands, 2005.
- Collenette, P. *The geology and Mineral Resources of the Pensiangan and Upper Kinabatangan Area, Sabah, Malaysia, Kuching*; Government Printing Office, Vincent Kiew Fah San: Sarawak, Malaysia, 1965.
- Alias, F.L.; Abdullah, W.H.; Hakimi, M.H.; Azhar, M.H.; Kugler, R.L. Organic geochemical characteristics and depositional environment of the Tertiary Tanjong Formation coals in the Pinangah area, onshore Sabah, Malaysia. *Int. J. Coal Geol.* **2012**, *104*, 9–21. [[CrossRef](#)]
- Thana'Ani, N.A.A.; Mustapha, K.A.; Idris, M. Source rock pyrolysis and bulk kinetic modelling of Miocene sedimentary sequences in southeastern Sabah, Malaysia: The variability of thermal maturity to oil-gas producing kerogen. *J. Pet. Sci. Eng.* **2022**, *208*, 109513. [[CrossRef](#)]
- Ayinla, H.A.; Abdullah, W.H.; Makeen, Y.M.; Abubakar, M.B.; Jauro, A.; Yandoka, B.M.S.; Abidin, N.S.Z. Petrographic and geochemical characterization of the Upper Cretaceous coal and mudstones of Gombe Formation, Gongola sub-basin, northern Benue trough Nigeria: Implication for organic matter preservation, paleodepositional environment and tectonic settings. *Int. J. Coal Geol.* **2017**, *180*, 67–82. [[CrossRef](#)]
- Berner, R.A. Sedimentary pyrite formation: An update. *Geochim. Et Cosmochim. Acta* **1984**, *48*, 605–615. [[CrossRef](#)]
- Naumann, D. Infrared spectroscopy in microbiology. *Encycl. Anal. Chem.* **2000**, *102*, 131.
- Çelik, Y.; Karayigit, A.I.; Oskay, R.G.; Kayseri-Özer, M.S.; Christanis, K.; Hower, J.C.; Querol, X. A multidisciplinary study and palaeoenvironmental interpretation of middle Miocene Keles lignite (Harmançık Basin, NW Turkey), with emphasis on syngenetic zeolite formation. *Int. J. Coal Geol.* **2021**, *237*, 103691. [[CrossRef](#)]
- Georgakopoulos, A. Study of Low Rank Greek Coals Using FTIR. *Energy Sources* **2003**, *25*, 995–1005. [[CrossRef](#)]
- Oikonomopoulos, I.K.; Perraki, M.; Tougiannidis, N.; Perraki, T.; Frey, M.J.; Antoniadis, P.; Ricken, W. A comparative study on structural differences of xylite and matrix lignite lithotypes by means of FT-IR, XRD, SEM and TGA analyses: An example from the Neogene Greek lignite deposits. *Int. J. Coal Geol.* **2013**, *115*, 1–12. [[CrossRef](#)]
- Loboziak, S.; Melo, J.H.G.; Stree, M. Devonian Palynostratigraphy in Western Gondwana. In *Applied Stratigraphy*; Springer: Berlin/Heidelberg, Germany, 2005; pp. 73–99.
- MacDonald, M.G. Methods in Quaternary Ecology # 2 Palynology. *Geosci. Can.* **1990**, *15*, 37–52.
- McCabe, P.J. Sedimentary Organic of Coal and Coal-Bearing Sequences. *Spec. Publ. Int. Assoc. Sedimentol.* **1984**, *7*, 13–42.
- Tyson, R.V. *Sedimentary Organic Matter (Organic Facies and Palynofacies)*; Springer: Dordrecht, The Netherlands; Chapman & Hall: London, UK, 1995; p. 615.
- Tongkul, F. Tectonic evolution of Sabah, Malaysia. *J. Southeast Asian Earth Sci.* **1991**, *6*, 395–405. [[CrossRef](#)]
- Hutchison, C.S. *Geological Evolution of South-East Asia*; Oxford University Press: Oxford, UK, 2007.
- Clennell, B. The origin and tectonic significance of mélanges in Eastern Sabah, Malaysia. *J. Southeast Asian Earth Sci.* **1991**, *6*, 407–429. [[CrossRef](#)]
- Tongkul, F. Structural styles, and tectonics of Western and Northern Sabah. *Bull. Geol. Soc. Malays.* **1990**, *27*, 227–240. [[CrossRef](#)]

21. Noad, J. The Sedimentology of the Mio-Pliocene Clastic Deposits of Eastern Sabah and Implications for Offshore Hydrocarbon Potential. *War. Geol.* **2003**, *29*, 19.
22. Friedrich, T.; Timmermann, A.; Tigchelaar, M.; Timm, O.E.; Ganopolski, A. Nonlinear climate sensitivity and its implications for future greenhouse warming. *Sci. Adv.* **2016**, *2*, e1501923. [[CrossRef](#)] [[PubMed](#)]
23. Moss, S.J.; Chambers, J.L. Tertiary facies architecture in the Kutai Basin, Kalimantan, Indonesia. *J. Asian Earth Sci.* **1999**, *17*, 157–181. [[CrossRef](#)]
24. Tongkul, F. The Paleogene basins of Sabah, East Malaysia. *Bull. Geol. Soc. Malays.* **1995**, *37*, 301–308. [[CrossRef](#)]
25. Clennell, B. *Far-Field and Gravity Tectonics in Miocene Basins of Sabah, Malaysia*; Geological Society: London, UK, 1996; Volume 106, pp. 307–320.
26. Hutchison, C.S.; Bergman, S.C.; Swauger, J.E. A Miocene collisional belt in north Borneo: Uplift mechanism and isostatic adjustment quantified by thermochronology. *J. Geol. Soc.* **2000**, *157*, 783–794. [[CrossRef](#)]
27. Balaguru, A.; Hall, R. Tectonic evolution and sedimentation of Sabah, North Borneo, Malaysia. *AAPG Search Discov. Artic.* **2008**, *30084*.
28. Lunt, P.; Madon, M. Onshore to offshore correlation of northern Borneo; a regional perspective. *Bull. Geol. Soc. Malays.* **2017**, *64*, 101–122. [[CrossRef](#)]
29. Wang, P.C.; Li, S.Z.; Guo, L.L.; Jiang, S.H.; Somerville, I.D.; Zhao, S.J.; Zhu, B.D.; Chen, J.; Dai, L.M.; Suo, Y.H.; et al. Mesozoic and Cenozoic accretionary orogenic processes in Borneo and their mechanisms. *Geol. J.* **2016**, *51*, 464–489. [[CrossRef](#)]
30. Collinson, J.D. The sedimentology of the Grindslow shales and the Kinderscout grit; a deltaic complex in the Namurian of Northern England. *J. Sediment. Res.* **1969**, *39*, 194–221. [[CrossRef](#)]
31. Maliva, R.G. *Aquifer Characterization Techniques*; Springer: Berlin/Heidelberg, Germany, 2016.
32. Miall, A.D. *The Geology of Fluvial Deposits*; Springer: Berlin/Heidelberg, Germany, 2006.
33. Painter, P.C.; Snyder, R.W.; Starsinic, M.; Coleman, M.M.; Kuehn, D.W.; Davis, A. Concerning the Application of FT-IR to the Study of Coal: A Critical Assessment of Band Assignments and the Application of Spectral Analysis Programs. *Appl. Spectrosc.* **1981**, *35*, 475–485. [[CrossRef](#)]
34. Tyson, R.V. Abundance of Organic Matter in Sediments: TOC, Hydrodynamic Equivalence, Dilution and Flux Effects. In *Sedimentary Organic Matter*; Springer: Berlin/Heidelberg, Germany, 1995; pp. 81–118.
35. Wood, D.G.; Gabriel, A.M.; Lawson, J.C. Palynological techniques—processing and microscopy. *AASP Found.* **1996**, *1*, 29–50.
36. Lowe, D.R. Sediment gravity flows; II, Depositional models with special reference to the deposits of high-density turbidity currents. *J. Sediment. Res.* **1982**, *52*, 279–297.
37. Mutti, E.; Davoli, G. *Turbidite Sandstones*; AGIP—Istituto di Geologia: Università di Parma, Italy, 1992.
38. Sumner, E.J.; Amy, L.A.; Tallin, P.J. Deposit Structure and Processes of Sand Deposition from Decelerating Sediment Suspensions. *J. Sediment. Res.* **2008**, *78*, 529–547. [[CrossRef](#)]
39. Buatois, L.A.; Mángano, M.G. Sedimentary facies, depositional evolution of the Upper Cambrian–Lower Ordovician Santa Rosita formation in northwest Argentina. *J. S. Am. Earth Sci.* **2003**, *16*, 343–363. [[CrossRef](#)]
40. Yoshida, M.; Rai, S.M.; Gajurel, A.P.; Bhattarai, T.N.; Upreti, B.N. Relationship between the Higher Himalayan Crystalline and Tethyan Sediments in the Kali Gandaki area, western Central Nepal: South Tibetan Detachment revisited. *Himal. J. Sci.* **2004**, *2*, 285. [[CrossRef](#)]
41. Boggs, S. *Principles of Sedimentology and Stratigraphy*; Pearson Prentice Hall: Upper Saddle River, NJ, USA, 2006; p. 581.
42. Reineck, H.-E.; Singh, I.B. Tidal Flats. In *Depositional Sedimentary Environments*; Springer: Berlin/Heidelberg, Germany, 1980; pp. 430–456.
43. Walker, R.G. Facies, facies models and modern stratigraphic concepts. In *Facies Models: Response to Sea Level Change*; Geological Association of Canada: St. John's, NL, Canada, 1992.
44. Howell, J.A.; Skorstad, A.; MacDonald, A. Sedimentological parameterization of shallow-marine reservoirs. *Pet. Geosci.* **2008**, *14*, 17–34. [[CrossRef](#)]
45. Hampson, G.J.; Gani, M.R.; Sharman, K.E.; Irfan, N.; Bracken, B. Along-Strike and Down-Dip Variations in Shallow-Marine Sequence Stratigraphic Architecture: Upper Cretaceous Star Point Sandstone, Wasatch Plateau, Central Utah, USA. *J. Sediment. Res.* **2011**, *81*, 159–184. [[CrossRef](#)]
46. Bhattacharya, J.P. Deltas. In *Facies Models 4*; James, N.P., Dalrymple, R.W., Eds.; Geological Association of Canada: St. John's, NL, Canada, 2010; pp. 232–264.
47. Retallack, G.J. Cenozoic Expansion of Grasslands and Climatic Cooling. *J. Geol.* **2001**, *109*, 407–426. [[CrossRef](#)]
48. Collinson, J.D. Alluvial Sediments. In *Sedimentary Environments: Processes, Facies and Stratigraphy*; Blackwell Science: Oxford, UK, 1996; pp. 37–81.
49. Anderton, R. Clastic facies models and facies analysis. In *Geological Society*; Special Publications: London, UK, 1985; Volume 18, pp. 31–47.
50. Ékes, C. Bedload-transported pedogenic mud aggregates in the Lower Old Red Sandstone in southwest Wales. *J. Geol. Soc.* **1993**, *150*, 469–471. [[CrossRef](#)]
51. Miall, A.D. Alluvial Models. In *Facies Models Response to Sea Level Change*; Geological Association of Canada: St. John's, NL, Canada, 1992; pp. 119–142.
52. Thomas, R.G.; Smith, D.G.; Wood, J.M.; Visser, J.; Calverley-Range, E.A.; Koster, E.H. Inclined heterolithic stratification—Terminology, description, interpretation and significance. *Sediment. Geol.* **1987**, *53*, 123–179. [[CrossRef](#)]

53. Buatois, L.A.; Santiago, N.; Herrera, M.; Plink-Bjorklund, P.; Steel, R.; Espin, M.; Parra, K. Sedimentological and ichnological signatures of changes in wave, river and tidal influence along a Neogene tropical deltaic shoreline. *Sedimentology* **2012**, *59*, 1568–1612. [[CrossRef](#)]
54. Miall, A.D. Lithofacies Types and Vertical Profile Models in Braided River Deposits: A Summary. *Fluv. Sedimentol.* **1977**, *5*, 597–604.
55. Miall, A.D. Tectonic setting and syndepositional deformation of molasse and other nonmarine-paralic sedimentary basins. *Can. J. Earth Sci.* **1978**, *15*, 1613–1632. [[CrossRef](#)]
56. Morley, R. Cenozoic ecological history of South East Asian peat mires based on the comparison of coals with present day and Late Quaternary peats. *J. Limnol.* **2013**, *72*, 36–59. [[CrossRef](#)]
57. Morley, R.J. Palynology of Tertiary and Quaternary Sediments in Southeast Asia. In *6th Annual Convention Proceedings*; Indonesian Petroleum Association: Jakarta, Indonesia, 1977.
58. Diessel, C.F.K. Coal Facies and Depositional Environment. In *Coal-Bearing Depositional Systems*; Springer: Berlin/Heidelberg, Germany, 1992; pp. 161–264.
59. Roberts, L.N.R.; McCabe, P.J. Peat accumulation in coastal-plain mires: A model for coals of the Fruitland Formation (Upper Cretaceous) of southern Colorado, USA. *Int. J. Coal Geol.* **1992**, *21*, 115–138. [[CrossRef](#)]
60. Scott, A.C. Observations on the nature and origin of fusain. *Int. J. Coal Geol.* **1989**, *12*, 443–475. [[CrossRef](#)]
61. De Vries Klein, G. Tidal circulation model for deposition of clastic sediment in epeiric and mioclinal shelf seas. *Sediment. Geol.* **1977**, *18*, 1–12. [[CrossRef](#)]
62. Van Wagoner, J.C.; Mitchum, R.M.; Campion, K.M.; Rahmanian, V.D. *Siliciclastic Sequence Stratigraphy in Well Logs, Cores, and Outcrops: Concepts for High-Resolution Correlation of Time and Facies*; The American Association of Petroleum Geologists: Tulsa, OK, USA, 1990.
63. Dalrymple, R.W.; Mackay, D.A.; Ichaso, A.A.; Choi, K.S. Processes, Morphodynamics, and Facies of Tide-Dominated Estuaries. In *Principles of Tidal Sedimentology*; Springer: Berlin/Heidelberg, Germany, 2012; pp. 79–107.
64. MacKay, D.A.; Dalrymple, R.W. Dynamic Mud Deposition in a Tidal Environment: The Record of Fluid-Mud Deposition in the Cretaceous Bluesky Formation, Alberta, Canada. *J. Sediment. Res.* **2011**, *81*, 901–920. [[CrossRef](#)]
65. Shiers, M.N.; Mountney, N.P.; Hodgson, D.M.; Cobain, S.L. Depositional controls on tidally influenced fluvial successions, Neslen Formation, Utah, USA. *Sediment. Geol.* **2014**, *311*, 1–16. [[CrossRef](#)]
66. MacEachern, J.A.; Bann, K.L. The Role of Ichnology in Refining Shallow Marine Facies Models. In *Recent Advances in Models of Siliciclastic Shallow-Marine Stratigraphy*; SEPM Special Publication: Tulsa, OK, USA, 2008.
67. Dalrymple, R.W.; Choi, K. Morphologic and facies trends through the fluvial–marine transition in tide-dominated depositional systems: A schematic framework for environmental and sequence-stratigraphic interpretation. *Earth-Sci. Rev.* **2007**, *81*, 135–174. [[CrossRef](#)]
68. Ichaso, A.A.; Dalrymple, R.W. Tide- and wave-generated fluid mud deposits in the Tilje Formation (Jurassic), offshore Norway. *Geology* **2009**, *37*, 539–542. [[CrossRef](#)]
69. Shelukhina, O.I.; El-Ghali, M.A.K.; Abbasi, I.A.; Khan, J.A.; Khalifa, M.K.; Rajendran, S.; Al-Sayigh, A. Facies architecture and depositional model for a fine-grained hybrid-energy delta: An example from the Upper Cambrian to Lower Ordovician Barik Formation, Central Oman. *Geol. J.* **2021**, *56*, 4254–4279. [[CrossRef](#)]
70. Berné, S.; Vagner, P.; Guichard, F.; Lericolais, G.; Liu, Z.; Trentesa, A. Pleistocene forced regressions and tidal sand ridges in the East China Sea. *Mar. Geol.* **2002**, *188*, 293–315. [[CrossRef](#)]
71. Yang, C.-S. Active, moribund and buried tidal sand ridges in the East China Sea and the Southern Yellow Sea. *Mar. Geol.* **1989**, *88*, 97–116. [[CrossRef](#)]
72. Dott, R.H.; Bourgeois, J. Hummocky stratification: Significance of its variable bedding sequences. *GSA Bull.* **1982**, *93*, 663–680. [[CrossRef](#)]
73. Duke, W.L. Hummocky cross-stratification, tropical hurricanes, and intense winter storms. *Sedimentology* **1985**, *32*, 167–194. [[CrossRef](#)]
74. Hampson, G.J. Sediment dispersal and quantitative stratigraphic architecture across an ancient shelf. *Sedimentology* **2010**, *57*, 96–141. [[CrossRef](#)]
75. Reinson, G.E. Barrier Island and Associated Strand-Plain Systems. In *Facies Models*; Geoscience Canada: Burnaby, BC, Canada, 1984; pp. 119–140.
76. Coates, J. Interpretation of Infrared Spectra, A Practical Approach. In *Encyclopedia of Analytical Chemistry*; John Wiley & Sons Ltd: Chichester, UK, 2000; pp. 10815–10837.
77. Öztaş, N.A.; Yürüm, Y. Pyrolysis of Turkish Zonguldak bituminous coal. Part 1. Effect of mineral matter. *Fuel* **2000**, *79*, 1221–1227. [[CrossRef](#)]
78. Volkov, D.S.; Rogova, O.B.; Proskurnin, M.A. Organic Matter and Mineral Composition of Silicate Soils: FTIR Comparison Study by Photoacoustic, Diffuse Reflectance, and Attenuated Total Reflection Modalities. *Agronomy* **2021**, *11*, 1879. [[CrossRef](#)]
79. Madejová, J. FTIR techniques in clay mineral studies. *Vib. Spectrosc.* **2003**, *31*, 1–10. [[CrossRef](#)]
80. Calderón, F.J.; Reeves, J.B.; Collins, H.P.; Paul, E.A. Chemical Differences in Soil Organic Matter Fractions Determined by Diffuse-Reflectance Mid-Infrared Spectroscopy. *Soil Sci. Soc. Am. J.* **2011**, *75*, 568–579. [[CrossRef](#)]

81. Changwen, D.; Jing, D.; Jianmin, Z.; Huoyan, W.; Xiaoqin, C. Characterization of Greenhouse Soil Properties Using Mid-Infrared Photoacoustic Spectroscopy. *Int. J. Rapid Commun.* **2011**, *44*, 359–368. [[CrossRef](#)]
82. Changwen, D.; Jianmin, Z.; Goynes, K.W. Organic and Inorganic Carbon in Paddy Soil as Evaluated by Mid-Infrared Photoacoustic Spectroscopy. *PLoS ONE* **2012**, *7*, e43368. [[CrossRef](#)]
83. Mathews, R.P.; Singh, B.D.; Singh, H.; Singh, V.P.; Singh, A. Characterization of Panandhro Lignite Deposits (Kachchh Basin), western India: Results from the Bulk Geochemical and Palynofloral Compositions. *J. Geol. Soc. India* **2018**, *91*, 281–289. [[CrossRef](#)]
84. Mustapha, K.A.; Abdullah, W.H.; Konjing, Z.; Gee, S.S.; Korai, A.M. Organic geochemistry and palynology of coals and coal-bearing mangrove sediments of the Neogene Sandakan Formation, Northeast Sabah, Malaysia. *Catena* **2017**, *158*, 30–45. [[CrossRef](#)]
85. Sykes, R. Depositional and Rank Controls on the Petroleum Potential of Coaly Source Rocks. In *PESA Eastern Australasian Basins Symposium*; Petroleum Exploration Society of Australia Special Publication: Melbourne, Australia, 2001.
86. Sykes, R. Peat biomass and early diagenetic controls on the paraffinic oil potential of humic coals, Canterbury Basin, New Zealand. *Pet. Geosci.* **2004**, *10*, 283–303. [[CrossRef](#)]
87. Sachsenhofer, R.F.; Privalov, V.A.; Izart, A.; Elie, M.; Kortensky, J.; Panova, E.A.; Sotirov, A.; Zhykalyak, M.V. Petrography and geochemistry of Carboniferous coal seams in the Donets Basin (Ukraine): Implications for paleoecology. *Int. J. Coal Geol.* **2003**, *55*, 225–259. [[CrossRef](#)]
88. Emerson, S.; Hedges, J.I. Processes controlling the organic carbon content of open ocean sediments. *Paleoceanogr. Paleoclimatol.* **1988**, *3*, 621–634. [[CrossRef](#)]
89. Meyers, P.A. Preservation of elemental and isotopic source identification of sedimentary organic matter. *Chem. Geol.* **1994**, *114*, 289–302. [[CrossRef](#)]
90. Painter, P.; Starsinic, M.; Coleman, M. Determination of Functional Groups in Coal by Fourier Transform Interferometry. In *Fourier Transform Infrared Spectra: Applications to Chemical Systems*; Academic Press, Inc.: London, UK, 1985; pp. 169–240.
91. Solomon, P.R.; Carangelo, R.M. FT-ir. analysis of coal: 2. Aliphatic and aromatic hydrogen concentration. *Fuel* **1988**, *67*, 949–959. [[CrossRef](#)]
92. Brown, J.M.; Elliott, J.J. Quantitative analysis of minerals in oil shales by fourier transform infrared spectroscopy. In *American Chemical Society*; Division of Petroleum Chemistry: Denver, CO, USA, 1987.
93. Charsky, A.; Herron, M.M. Quantitative analysis of kerogen content and mineralogy in shale cuttings by Diffuse Reflectance Infrared Fourier Transform Spectroscopy. In Proceedings of the International Symposium, Society of Core Analysts, Aberdeen, UK, 27–30 August 2012.
94. Matteson, A.; Herron, M.M. Quantitative mineral analysis by Fourier Transform Infrared Spectroscopy. In Proceedings of the International Symposium, Society of Core Analysts, Aberdeen, UK, 27–30 August 2012.
95. Van der Marel, H.W.; Beutelspacher, H. *Atlas of Infrared Spectroscopy of Clay Minerals and Their Admixtures*; Elsevier: Amsterdam, The Netherlands, 1976.
96. Pironon, J.; Pelletier, M.; de Donato, P.; Mosser-Ruck, R. Characterization of smectite and illite by FTIR spectroscopy of interlayer NH₄⁺ cations. *Clay Miner.* **2003**, *38*, 201–211. [[CrossRef](#)]
97. Palayangoda, S.S.; Nguyen, Q.P. An ATR-FTIR Procedure for Quantitative Analysis of Mineral Constituents and Kerogen in Oil Shale. *Oil Shale* **2012**, *29*, 344–356. [[CrossRef](#)]
98. Krivoshein, P.K.; Volkov, D.S.; Rogova, O.B.; Proskurnin, M.A. FTIR photoacoustic spectroscopy for identification and assessment of soil components: Chernozems and their size fractions. *Photoacoustics* **2020**, *18*, 100162. [[CrossRef](#)]
99. Inoue, A.; Watanabe, T. Infrared Spectra of Interstratified Illite/Smectite from Hydrothermally Altered Tuffs (Shinzan, Japan) and Diagenetic Bentonites (Kinnekulle, Sweden). *Clay Sci.* **1989**, *7*, 263–275.
100. Max, J.-J.; Chapados, C. Isotope effects in liquid water by infrared spectroscopy. III. H₂O and D₂O spectra from 6000 to 0 cm⁻¹. *J. Chem. Phys.* **2009**, *131*, 184505. [[CrossRef](#)]
101. Slaný, M.; Jankovič, L.; Madejová, J. Structural characterization of organo-montmorillonites prepared from a series of primary alkylamines salts: Mid-IR and near-IR study. *Appl. Clay Sci.* **2019**, *176*, 11–20. [[CrossRef](#)]
102. Terra, F.S.; Demattê, J.A.; Rossel, R.A.V. Spectral libraries for quantitative analyses of tropical Brazilian soils: Comparing vis-NIR and mid-IR reflectance data. *Geoderma* **2015**, *255–256*, 81–93. [[CrossRef](#)]
103. Stevenson, F.J. Extraction, fraction, and general chemical composition of soil organic matter. In *Humus Chemistry: Genesis, Composition, Reactions*; John Wiley & Sons, Inc: New York, NY, USA, 1994; pp. 24–56.
104. Daidu, F.; Yuan, W.; Min, L. Classifications, sedimentary features and facies associations of tidal flats. *J. Palaeogeogr.* **2013**, *2*, 66–80.
105. Monga, P.; Kumar, M.; Prasad, V.; Joshi, Y. Palynostratigraphy, palynofacies and depositional environment of a lignite-bearing succession at Surkha Mine, Cambay Basin, north-western India. *Acta Palaeobot.* **2015**, *55*, 183–207. [[CrossRef](#)]
106. Paul, S.; Sharma, J.; Singh, B.D.; Saraswati, P.K.; Dutta, S. Early Eocene equatorial vegetation and depositional environment: Biomarker and palynological evidences from a lignite-bearing sequence of Cambay Basin, western India. *Int. J. Coal Geol.* **2015**, *149*, 77–92. [[CrossRef](#)]

Disclaimer/Publisher's Note: The statements, opinions and data contained in all publications are solely those of the individual author(s) and contributor(s) and not of MDPI and/or the editor(s). MDPI and/or the editor(s) disclaim responsibility for any injury to people or property resulting from any ideas, methods, instructions or products referred to in the content.